Dendritic-cell diversity in equine blood revealed by single-cell transcriptomics

Ambre Baillou[1,2], Marius Botos[1,2], Simone Oberhaensli[3†], Iva Cvitas[4††], Sigridur Jonsdottir[4†††], Anja Ziegler[4††††], Francisco Brito[1,2], Artur Summerfield[1,2], Eliane Marti[4], Stephanie C. Talker[1,2]

[1]*Institute of Virology and Immunology, Bern, Switzerland*
[2]*Department of Infectious Diseases and Pathobiology, Vetsuisse Faculty, University of Bern, Bern, Switzerland*
[3]*Interfaculty Bioinformatics Unit and Swiss Institute of Bioinformatics, University of Bern, Bern, Switzerland*
[4]*Department of Clinical Research and Veterinary Public Health, Vetsuisse Faculty, University of Bern, Bern, Switzerland*

[†] *present affiliation: Next Generation Sequencing Platform and Institute for Fish and Wildlife Health, Vetsuisse Faculty, University of Bern, Bern, Switzerland*
[††] *present affiliation: Institute of Animal Pathology, Vetsuisse Faculty, University of Bern, Bern , Switzerland*
[†††] *present affiliation: Institute for Experimental Pathology, Biomedical Center, University of Iceland, Keldur, Reykjavik, Iceland and Faculty of Medicine, University of Iceland, Reykjavik, Iceland*
[††††] *present affiliation: LaboRvet AG, Reiden, Switzerland*

Corresponding author:
Stephanie Talker
Länggassstrasse 122, 3012 Bern, Switzerland
Tel: +41 31 684 2483
stephanie.talker@unibe.ch

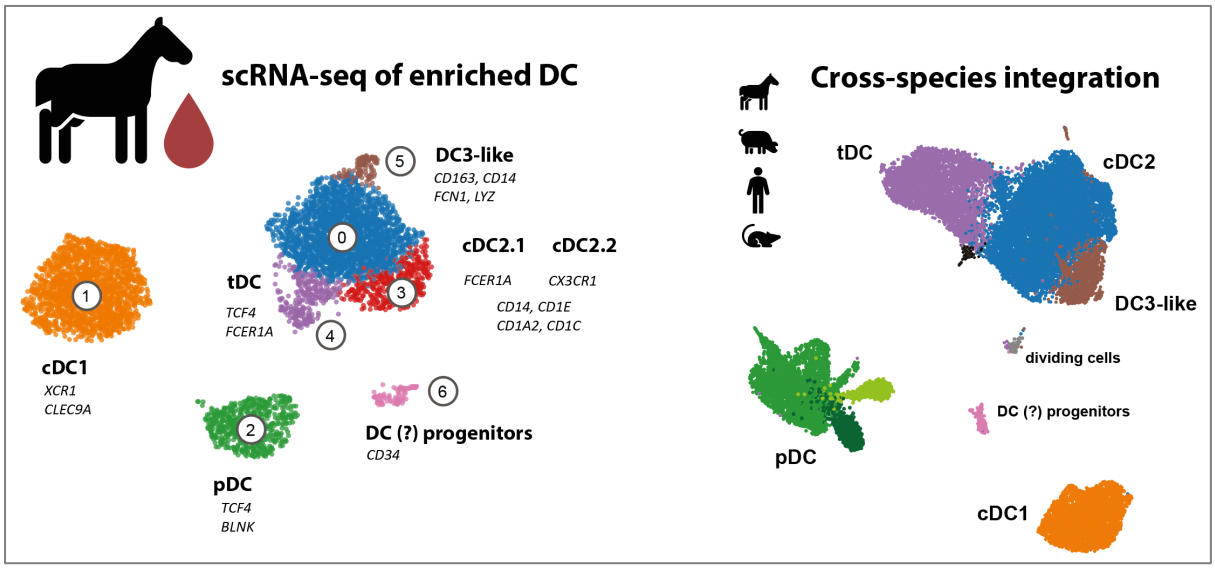

ABSTRACT

Unbiased classification of equine dendritic cells (DC) is necessary to address various research questions such as the role of DC subsets in immune-mediated diseases of horses. We applied single-cell RNA sequencing (scRNA-seq) on DC enriched from the blood of two horses. All main DC subsets were detected by key gene expression, including conventional DC type 1 (cDC1; *XCR1*) and type 2 (cDC2; *FCER1A*, *CD1E*) as well as plasmacytoid DC (pDC; *TCF4*). In addition, we detected a small cluster of hematopoietic progenitors, as well as transitional DC (tDC; *FCER1A*, *TCF4*) and putative DC type 3 (DC3; *FLT3*, *CD163*). Our data confirms the previously reported phenotype of equine pDC (Flt3^{+}MHC-II^{low}CADM1^{low}CD172a^{int}), cDC1 (Flt3^{+}MHC-II^{high}CADM1^{high}CD172a$^{low-int}$) and cDC2 (Flt3^{+}MHC-II^{high}CADM1^{int}CD172a^{high}), while also highlighting considerable CD14 expression for cDC2. Two subclusters of equine cDC2 were found to be enriched in *FCER1A* or *CX3CR1* transcripts (cDC2.1 and cDC2.2, respectively), with suggested enhanced extravasation and T-cell stimulatory capacities of the latter. Conservation of DC subsets across species (horse, pig, human, mouse) was illustrated by enrichment analyses with subset-specific gene signatures and by cross-species data integration with publicly available scRNA-seq datasets. Our atlas of equine blood DC is a valuable resource for comparative analyses, and it forms the foundation for understanding the involvement of distinct DC subsets in infections and immune-mediated pathologies.

Key words: equine blood dendritic cells, single-cell RNA-seq, cDC1, cDC2 subsets, pDC, tDC, DC3

INTRODUCTION

Dendritic cells (DC), despite their low frequency in tissues and blood, are central players in the immune system, initiating and fine-tuning adaptive immune responses (1). Traditionally, DC have been classified as conventional DC (cDC) and plasmacytoid DC (pDC). Conventional DC are grouped into two main subtypes: cDC1, specialized in cross-presenting antigens through MHC class I molecules, enabling them to prime CD8 T cells, and cDC2, known to be specialized in promoting Th2 and Th17 responses (2). While the antigen presenting capabilities of pDC are being debated, they are known for their potent antiviral effect by rapidly producing type I interferon (3), including horse (4). Flow cytometry (FCM) is widely employed for the characterization of DC subsets across species (5). However, in contrast to human and mouse, studies in veterinary species face several challenges such as limited availability of species-reactive and fluorochrome-coupled monoclonal antibodies (6). Furthermore, capturing the full spectrum of

DC diversity and plasticity by a set of pre-defined markers in FCM is not feasible and prone to bias. Single-cell RNA-sequencing (scRNA-seq) has enabled the identification of novel DC subsets, including DC type 3 (DC3) (7,8) and transitional DC (tDC) in human (9), mouse (10–12), and pig (13). Across species investigated so far, DC3 have been described to share transcriptomic signatures with both cDC2 and monocytes (11,14), reflecting their origin from monocyte-dendritic-cell progenitors (7,11,15). In contrast, tDC were shown to originate from pro-pDC and to differentiate into cDC2-like cells termed tDC2, with an improved ability to prime T cells, and to produce pro-inflammatory IL-1β (12). However, delineating cDC2 subsets, monocyte-like DC, and monocytes remains a challenging task due to overlapping phenotypes and transcriptomes. In horse, a scRNA-seq study of PBMC by Patel *et al.* confirmed the identification of cDC1, cDC2 and pDC in blood (16), but, due to the small number of detected DC, could not elaborate on DC heterogeneity

Here, we describe previously unreported heterogeneity of DC in equine blood. By enriching DC prior to scRNA-seq, we were able to detect four main DC subsets (cDC1, cDC2, pDC, tDC) alongside DC3-like cells and hematopoietic progenitors / putative DC progenitors. Enrichment analysis and cross-species integration further confirmed the transcriptional similarity of DC subsets across human, pig, mouse and horse.

RESULTS

Equine cDC1, cDC2 and pDC defined by expression of key genes

Equine DC were enriched using FACS from freshly isolated PBMC of three horses and subsequently processed for scRNA-seq. As defined by prior phenotyping (**Supp. Fig.1A**), DC were enriched by gating on Flt3^{+} cells, and the presence of monocytes in the sorting gate was further reduced by selecting cells that expressed higher levels of CADM1 (**Figure 1A, Supp. Fig. 1B**). Upon processing, scRNA-seq data of one horse was excluded from further analyses due to low number of cells (**Supp. Fig. 2A**). As shown in **Figure 1B**, scRNA-seq of enriched DC from the remaining two horses resulted in the detection of seven clusters (clustering resolution of 0.45).

By visualizing the expression of key marker genes, we identified cluster 6 as hematopoietic progenitors (*CD34*), cluster 1 as cDC1 (*XCR1*, *BATF3*, *IRF8*, *CLEC9A*, *CLNK*, *CADM1*), clusters 0, 3, 4, and 5 as cDC2-like cells (*FCER1A*, *CD1C*, *CD1A2*, *CSF1R*, *SIRPA*) and cluster 2 as pDC (*TCF4*, *BLNK*, *IRF7*, *SPIB*) (**Fig. 1B-D**). With 50% (Horse #1) and 60% (Horse #2), cDC2-like cells were found to be the most abundant cell type within enriched DC, followed by cDC1 (27% / 35%), pDC (22% / 5%) and hematopoietic progenitors (2% / 2%) **(Supp. Fig. 2B)**.

Differential expression analysis (DEA) revealed additional genes with enriched transcription in hematopoietic progenitors (e.g. *MEIS1*, *DACH1, ERG, KIT, IKZF2, MSI2),* cDC1 (e.g. *CPVL*, *CST3*, *LRRK2*, *ID2, RAB7B, DNASE1L3, CD8A*), cDC2-like cells (e.g. *S100A4*, *MNDA*, *GIMAP5*, *TYROBP, IFI16, IL32*) and pDC (e.g. *CTSC*, *UGCG*, *FYB1*, *CLECL1, PLAC8B*) (**Fig. 1E, Supp. Table 1**). Transcript detection for *FLT3, CD14, SIRPA* (*CD172a*)*, CADM1,* and *ELA-DRA* (MHC-II) in the cDC1, cDC2 and pDC clusters (**Fig. 1F**) was in line with surface protein expression detected by flow cytometry (**Supp. Fig. 1**) and with previous phenotyping reported by Ziegler *et al*. (4).

Delineation of transitional DC (tDC) and putative DC3 from cDC2

Among cDC2-like cells, four distinct clusters were apparent (**Fig. 2A**). Two clusters (c0 and c3) were in fact comprised of cDC2, as judging from their specific expression of *CD1E, CD1A2*, and *CD1C* (**Fig. 2B**). One cluster (c4) was identified as tDC according to its expression of pDC-associated genes (e.g. *TCF4*, *SPIB*, *BLNK*) (**Fig. 2C**) alongside cDC2-associated genes (*FCER1A*, *KLF4, MNDA*) (**Supp. Table 1**). Cluster 5 displayed a monocyte-like signature (e.g. *FCN1*, *S100A12*, *C5AR1*) (**Fig. 2D**). Based on co-expression of *FLT3* (DC marker) and *CSF1R* or *CD163* (monocyte-associated) (**Fig. 2E**), we annotated this cluster as putative DC3. Gene module scoring confirmed the inflammation-associated signature of the putative DC3 cluster and additionally revealed an enrichment of complement-associated transcripts (**Fig. 2F**). Notably, cells annotated as cDC2 (c0&c3, in particular c3) were enriched in MHC-II-associated transcripts (**Fig. 2G**).

Among the top gene transcripts enriched in tDC over cDC2 were *PLPP3* (regulator of bioactive lipids such as sphingosine-1-phosphate), *DPP4* (regulator of chemokine activity), *PLXNA4* (co-receptor for semaphorins), *CD5* (immunostimulatory receptor for effector T cell priming), *ENSECAG00000037376* (predicted ortholog of *CRLF2),* encoding a co-receptor for TSLP recently implicated in tDC2-mediated immunosuppression (17) *,* as well as several pDC-associated genes (e.g. *RUNX2*, *IRF8*, *IKZF1*, *PLAC8B*) (**Fig. 2H, Supp. Table 2**).

In line with their monocyte-like signature, putative DC3 contained higher levels of *TLR4*, *VCAN* and *F13A1* transcripts when compared to cDC2. Other top genes differentiating DC3 from cDC2 included e.g. *THBS1*, *PLD3* and *SELP*. Complete gene lists from DEA are provided as **Supplementary Table 2**.

Heterogeneity of cDC2

Two clusters of cDC2 were evident in our dataset (**Fig. 3A**; c0 and c3), referred to as cDC2.1 (c0) and cDC2.2 (c3). While cDC2.1 expressed higher levels of *FCER1A*, cDC2.2 were enriched in *CX3CR1* transcripts (**Fig. 3A**). Among the top differentially expressed genes in cDC2.1 (when

compared to cDC2.2) were transcripts associated with pro-inflammatory (*S100A4*, *CLEC5A*, *CTSB*) and regulatory (*CD52*, *CLEC12A*) functions, as well as pattern recognition (*CLEC1A*, *CLEC5A*, *TLR2*) (**Fig. 3B-C**, **Supp. Table 2**). Moreover, cDC2.1 appeared to have high translational activity, as suggested by high expression of ribosomal genes (**Fig. 3C**).

In contrast, cDC2.2 stood out by enrichment of extravasation-associated transcripts such as *PECAM1* and *ITGA4* and displayed a more mature transcriptome with capacity for modulation of T-cell responses, suggested by high expression of MHC-II- associated transcripts, *CD83* and *TIMD4* (**Fig. 3B-C**, **Supp. Table 2**). Notably, cDC2.2 contained considerably higher levels of *CD2* transcripts, making CD2 a potential marker to discriminate equine cDC2 subsets by flow cytometry.

Moreover, we found differences in the activity of certain pathways (**Fig. 3D**), most notably higher TNF-α activity in cDC2.1 vs. higher activity of NF-κB, MAPK, TRAIL and TGF-β in cDC2.2, with the latter two pathways potentially reflecting a more regulated state prone to apoptosis/ apoptosis induction and resolution of inflammation, altogether appearing more adapted for tissue infiltration.

Gene-ontology based over-representation analysis supported transcript enrichment for migration and antigen presentation in cDC2.2 (**Fig. 3E**). Inferred transcription factor activity further supported high metabolic activity in cDC2.1 (PPARGC1A) seemingly adapted to hypoxic environments (HIF1A), and prominent antigen presentation and T-cell stimulatory capabilities in cDC2.2 (CIITA, RARA) (**Fig. 3F**).

Notably, the signature of murine cDC2A was not clearly enriched in equine *CX3CR1*-expressing cDC2.2 compared to cDC2.1 (**Supp. Fig. 3**). This would suggest that CX3CR1 expression in equine cDC2 subsets cannot be used to differentiate putative analogs of the cDC2A and cDC2B subsets described for mouse and human.

Delineation of DC from monocytes

Precise delineation of cDC2 and DC3 from monocytes is challenging across species. As our DC-enriched dataset likely contains very few monocytes, we took advantage of a previously published scRNA-seq dataset generated from equine PBMC (16), denoted “Patel dataset”, to integrate our dataset with a dataset containing both equine DC and monocytes (**Fig. 4A**, **Supp. Fig. 4**).

We identified ten distinct clusters within the integrated dataset (**Fig. 4B**), with cDC1 and pDC clearly aligning across datasets (**Fig. 4C**). As expected, monocytes clustered with our DC3 (**Fig. 4C**) and originated mostly from the Patel dataset (**Fig. 4D**). As indicated by arrows in the lower

panel of **Figure 4E**, cDC2 from the Patel dataset clustered according to expression of *FCER1A* and *CX3CR1* (c2 and c7), thus corresponding to the cDC2 subsets described in our study (**Fig. 3**), and according to *TCF4* expression (c8), thus corresponding to tDC described in our study (**Fig. 2**). Notably, part of the *FCER1A*-expressing cDC2 contained in our dataset (cDC2.1 in **Fig. 4C**) clustered close to monocytes (Patel dataset) and DC3-like cells (own dataset) (**Fig. 4C**), but in contrast to them almost lacked detectable *LYZ* expression (**Fig. 4E**).

Overall, while c4 and c3 appeared to be enriched for cDC2 and monocytes, respectively **(Fig. 4F)**, both of these clusters also contained DC3-like cells, as indicated by shared expression of DC- and monocyte-associated genes (**Fig. 4G**).

Gene expression related to main DC functions

Genes associated with DC functions, such as pattern recognition, migration and adhesion, antigen presentation and T-cell modulation, as well as genes for other categories of interest, were visualized for all seven analyzed DC clusters (**Fig. 5A**).

Among genes encoding toll-like receptors, *TLR4 and TLR8* transcripts were almost exclusively detected in putative DC3, which were also enriched for *TLR1* and *TLR6* transcripts (**Fig. 5B**). Expression of *TLR9* was selectively found in pDC, and expression of *TLR3* mostly in cDC1 and to a lesser extent in hematopoietic progenitors. Transcripts of *TLR7* were enriched in both DC3 and pDC. Most notably, cDC1 stood out by high and specific expression of *TLR12*. Overall, TLR gene expression appeared to be comparably low in tDC, with most transcripts detected for *TLR1*, *TLR2*, *TLR5* and *TLR10*. Among pattern-recognition-receptor (PRR) genes clearly expressed in tDC were *CLEC4G*, *CLEC12A* and *AIM2*, with *CLEC4G* expression exclusively shared with pDC, *CLEC12A* expression shared with all subsets except for cDC1 and progenitors, and *AIM2* expression specifically absent from pDC and progenitors.

For other PRR-associated transcripts, we found exclusive enrichment in pDC (*NLRC3*, *CD209*), strong expression in DC3 (e.g. *NLRC5*, *NLRP3*, *CLEC1A*, *CLEC2B*, *FCN1*), and exclusive or considerably high expression in progenitors (*CLEC11A*, *SCARB1*, *RIGI*).

Looking at antigen presentation and T-cell modulation, expression of MHC-II-related genes was highest in cDC1 and cDC2.2 (**Fig. 5C**), while gene expression for CD1 molecules showed a more complex pattern: cDC2 expressed the highest levels of *CD1A2*, *CD1C* and *CD1E2*, while transcripts for *CD1A4* were enriched in cDC2.1 and DC3. Notably, transcripts for *CD1E1* were enriched in pDC, which also expressed considerable levels of *CD1C*. Expression of other CD1 genes (*CD1A3*, *CD1A6*, *CD1A7*, *CD1B2*, *CD1D*) was hardly detected in the present dataset. As

expected, *WDFY4* (involved in cross-presentation) showed the highest expression in cDC1. Notably, the second highest level for *WDFY4* was detected in pDC, followed by tDC and cDC2.2. Only transcripts for *CD200R1* (inhibitory receptor) were somewhat enriched ($\log_2$FC = 0.954) in tDC over other DC subsets.

Among genes encoding cytokines and cytokine receptors, pDC stood out by high expression of *IFNAR1*, *IFNLR1*, *IL10RB* and *TGFBR1/2* (**Fig. 5D**). Notably, cDC1 appeared to exclusively express *IL12RB2* and *IL21R* and shared high expression of *IL16* and *IL20RB-1* with cDC2.2. Expression of *IL1B* appeared to be higher in cDC2.1 than in cDC2.2, whereas cDC2.2 expressed higher levels of *IL2RG*, *IL6ST*, *IL16*, and *TGFB1* transcripts than cDC2.1. While tDC appeared to contain the highest levels of *IL17RA* transcripts, DC3 were enriched in transcripts of *IFNGR1/2*, *IL1R1*, *IL1RN*, *IL4R*, *IL15*, *IL15RA* and *IL18*.

Chemokine gene transcripts were mostly detected in DC3 (*CCL8*, *CXCL16*), alongside *CCR2*, *CCR5, and CCRL2* transcripts (**Fig. 5E**), which were also detectable in cDC2.1 at lower levels. Notably, pDC stood out by expression of *CXCR2*, *CXCR3* and *CXCR4*, while *CX3CR1* expression was highest in the cDC2.2 subset.

Looking at adhesion-associated gene expression, pDC, alongside tDC, expressed the highest levels of *SELL* (CD62L) and *ITGAL* (CD11a) (**Fig. 5F**). Notably, integrin-encoding transcripts were expressed in a highly subset-specific manner, with *ITGAE* (CD103), *ITGA7, ITGB3* and *ITGB7* clearly enriched in pDC, *ITGAM* (CD11b) and *ITGB5* in DC3, and *ITGA5* and *ITGA6* in hematopoietic progenitors.

Among genes encoding Fc receptors, tDC, alongside cDC2.1, expressed the highest levels of *FCER1A* transcripts, and shared *FCGRT* (FcRn) expression with the other cDC subsets (**Fig. 5G**). Expression of genes encoding B-cell associated Fc receptors (*FCMR*, *FCRLA*, *FCRL5*) was found to be highest in pDC. Notably, *FCMR* (encoding the Fc receptor for IgM) was the only gene in this group also clearly expressed in hematopoietic progenitors.

Looking at transcripts associated with the complement response, progenitors appeared to exclusively express *C7* (component of membrane-attack complex) and regulatory *CFI* (**Fig. 5H**), while pDC showed the highest expression of *C1QB* and *C1QBP* (initiation and regulation, respectively, of classical complement activation), and DC3 of regulatory *C4BPA* and chemotaxis/inflammation-mediating *C5AR1* (CD88). Transcripts encoding Properdin (*CFP*), binding to microbial surfaces and leading to alternative complement activation, showed the highest expression in cDC2.2 and were specifically absent from pDC and hematopoietic progenitors.

Species comparisons support identification of equine tDC and DC3

To explore the conservation of equine DC subsets across species, we first examined the relative enrichment of DC signatures from human blood (9), murine spleen (18) and porcine blood (13) in our equine scRNA-seq clusters (**Fig. 6A**) by gene set enrichment analysis (GSEA). Results were visualized using heatmaps (**Fig. 6B-D**), complemented by feature plots to examine the distribution of enrichment scores across clusters, with manually defined thresholds for each gene set (**Supp. Fig. 5**). Overall, pDC- and cDC1-derived signatures were specifically conserved between horse and compared species, as judged by high enrichment scores for analogous subsets (**Fig. 6B-D**, **Supp. Fig. 5**).

Signatures from human, porcine, and murine cDC2 showed the highest enrichment in equine cDC2 clusters, with notable enrichment detected also in equine DC3, particularly for one cluster of murine cDC2.

Notably, porcine and human tDC signatures showed the highest enrichment in equine tDC. Consistent with the reported cDC2-like and tDC-like profiles of porcine tDC clusters tDC.1 and tDC.2 (13), their signatures also showed enrichment in equine cDC2.2 and pDC clusters, respectively. Moreover, the porcine tDC.1 signature was considerably enriched in equine cDC1.

Murine tDC signatures were primarily enriched in equine cDC2.2 (murine tDC bulk), in equine cDC2.1 and DC3 (murine tDC^{low}), or in both equine cDC2.1 and cDC2.2 (murine tDC^{high}).

Porcine and human DC3 signatures resulted in the highest enrichment in the equine DC3 cluster, with additional – but comparatively lower – enrichment in the cDC2 clusters. A murine DC3 signature was not available from the mouse study we used for GSEA, but, as suggested above and further below, murine DC3 may be included within cDC2 clusters.

Next, we integrated DC-enriched scRNA-seq datasets from horse, pig, human, and mouse (**Fig. 6E**). For most species, integration resulted in co-clustering of subsets, supporting overall conservation of DC transcriptomes across species (**Fig. 6F-H**). An interesting finding was that equine cDC2.2 clustered with the porcine tDC.1 subset, echoing GSEA findings shown above, and highlighting the difficulty of clearly assigning an identity to these cell types. Notably, cells annotated as DC3 in the murine dataset clustered with cDC2 of other species (horse, pig, human), while cells annotated as pro-DC3 in the murine dataset clustered with DC3 across species. Cells annotated as pre-DC2 in the murine dataset clustered not only with cDC2 but also with tDC and pDC of the other species, likely reflecting additional heterogeneity in the previously annotated murine pre-DC2 cluster. The largest proportion of these cells annotated as murine pre-DC2 was found within the tDC cluster (c3) of the integrated dataset (**Supp. Fig. 6A**).

Expression of key genes was also largely conserved across species (**Supp. Fig. 6B**), with the notable exception of *FCER1A* and *FCN1*, which could not be detected in the murine dataset, and *F13A1*, which was highly expressed across porcine pDC and cDC2-like cells, but only detected in DC3 /proDC3 of the other species.

DISCUSSION

Our study provides the first in-depth analysis of equine DC heterogeneity at the single-cell transcriptomic level. By performing scRNA-seq on enriched Flt3^{+} DC from blood of two horses, we identified five DC subsets, including tDC and putative DC3 alongside cDC1, cDC2, and pDC. Equine cDC1 and pDC were detected as distinct clusters expressing key genes conserved across species. Equine cDC2-like cells formed the biggest cluster (approx. 50 % within DC) and could be separated into at least two cDC2 subsets, as well as putative DC3 and tDC.

The phenotype of equine DC has previously been studied by gating on Flt3^{+} PBMC, and equine pDC were identified as Flt3^{+}CADM1^{low}MHC-II^{low}, and confirmed by qPCR for conserved key genes (*PLAC8B*, *RUNX2*, *TCF4*) (4). Our scRNA-seq dataset validates this gating strategy and the described phenotype, with pDC expressing relatively low levels of CADM1 and MHC-II, and presumably lacking expression of CD172a and CD14. Putative cDC1 were described as Flt3^{+}CD4^{-}CD13^{+}CD172a^{-}CADM1^{high}MHC-II^{high}, which is in line with the high expression of *CADM1* and genes encoding MHC-II molecules in the cDC1 cluster of our scRNA-seq dataset. In the same study (4), putative cDC2 were described as Flt3^{+}CD4^{-}CD13^{-}CD172a^{high}CADM1^{int}MHC-II^{high} and were gated by excluding CD14^{+} cells. As discussed below, our data (scRNA-seq and flow cytometry) clearly show CD14 expression on equine cDC2 arguing for an adjusted gating strategy without excluding CD14^{+} cells, but instead taking the expression level of CADM1 into account.

Other groups have characterized equine immune cells by scRNA-seq of PBMC (16), BALF (bronchoalveolar lavage fluid) (19–21), synovial fluid (22), and endometrium (23), but detected only low frequencies of DC. For the present study, we aimed to enrich DC as much as possible and to exclude most monocytes by stringent gating on higher CADM1 expression within the Flt3 gate. While this enhanced enrichment of DC proved beneficial to detect rare progenitors and DC subsets like tDC and DC3, our gating strategy may also have excluded some cDC2 and DC3 from our analysis, as continuous CADM1 expression levels on CD14^{+} cells did not allow for a clear separation of dendritic and monocytic cells. This phenotypic overlap at the cDC2/DC3/monocyte interface is encountered across species, making a clear separation of these subsets challenging – even at the single-cell transcriptomic level. This was also evident in our attempt to delineate DC3 and cDC2 from monocytes by integration with previously published scRNA-seq data that

292 include equine monocytes (16). Sequencing of enriched DC alongside total mononuclear
293 phagocytes from the same sample should minimize confounding batch effects and provide a
294 more accurate picture of cDC2 vs. monocyte identity. However, a clear delineation of DC3 will
295 likely remain challenging, as shown in our recently published DC atlas for blood of pigs (13).
296 Expression of CX3CR1 distinguishes murine T-bet$^-$ cDC2 (cDC2B) from T-bet$^+$ cDC2 (cDC2A) (24).
297 At first glance, the two cDC2 clusters identified in our dataset (termed here cDC2.1 and cDC2.2)
298 resembled CX3CR1-defined cDC2 subsets described in human and mouse (25). However, equine
299 signatures don't fit to the reported dichotomy of pro-inflammatory CX3CR1$^+$ cDC2 and pro-
300 resolving CX3CR1$^-$ cDC2.
301 Rather, equine cDC2.1 (lacking *CX3CR1* expression while expressing *CCR2*) appear to be
302 metabolically active with a relatively pro-inflammatory signature (e.g. high *IL1B* transcription),
303 and cDC2.2 (expressing *CX3CR1* while lacking *CCR2* expression) seem to be specialized in
304 extravasation and antigen presentation. Differential gene expression analysis revealed additional
305 potentially interesting transcripts, such as CD52 (higher in cDC2.1) and TIMD4 (higher in cDC2.2).
306 While CD52 expression on DC has been proposed to be downregulated upon extravasation into
307 tissues (26), TIMD4 has been reported to be upregulated upon activation of DC and to promote T-
308 cell expansion and survival (27) alongside efferocytosis. Although highly speculative, this would
309 support the idea that cDC2.2 represent a more differentiated version of cDC2.1 that down-
310 regulate CD52 while upregulating TIMD4 among other co-stimulators (e.g. CD83), ready to enter
311 tissues, in order to support effector T cells.
312 Notably, CX3CR1 expression appears to also distinguish two subsets of bovine blood cDC2, as
313 suggested by flow cytometry (28), and future scRNA-seq data of enriched bovine DC will provide
314 a valuable resource for cross-species analyses on CX3CR1-defined cDC2 heterogeneity.
315 Although cDC2 heterogeneity, presumably shaped by ontogeny (29,30) as well as environmental
316 plasticity (31), will likely remain challenging to dissect – across species and tissues (32). A subset
317 of inflammatory cDC2 described in humans (33) was later discovered to comprise a separate DC
318 lineage: DC3, characterized by co-expression of dendritic and monocytic markers, such as CD14
319 (11,15). Across species, expression of CD14 is used to identify monocytes and to differentiate
320 them from DC (2,34,35). With the discovery of *CD14*-expressing DC3 in human and mouse
321 (7,8,11,14), this marker has been put into question. In pig, *CD14* expression appears to be
322 similarly limited to DC3 and monocytes (13), however, our scRNA-seq data and additional
323 phenotyping data now clearly indicate that equine cDC2 express considerable levels of CD14 and
324 that, instead of CD14, expression of CD163 in combination with Flt3 may be suitable for

distinguishing DC3 (Flt3^{+}CD163^{+}) from cDC2 (Flt3^{+}CD163^{-}) and monocytes (Flt3^{-}CD163$^{+/-}$) in horses.

Identification of tDC was based on expression of pDC-associated genes (*TCF4*, *SPIB*, *BLNK, PLAC8B*) alongside cDC2-associated genes like *FCER1A*. This transcriptomic signature shared between pDC and cDC2 is described across species investigated so far, including human (9), mouse (12), and more recently pig (13), and supports their proposed origin from pro-pDC and differentiation towards cDC2-like cells (12).

In terms of function, tDC have been described to produce pro-inflammatory IL1-β during viral infection in the mouse model (12), and to be recruited to human skin upon experimental inoculation with UV-inactivated *E. coli* (36). High levels of *IL1B* transcripts were specifically detected in equine cDC2, and to a much lesser extent in tDC. Moreover, compared to other DC subsets, overall expression of TLR genes was found to be low in equine tDC. Nevertheless, the detected gene transcripts support their involvement in bacterial recognition (*TLR1*, *TLR2, TLR5*) and regulation of inflammation (*TLR10*). In mouse models of skin inflammation and cancer, tDC-derived tDC2 were recently reported to induce regulatory T cells when sensing thymic stromal lymphopoietin (TSLP), thereby promoting immunosuppression (17). Equine tDC expressed the predicted equine ortholog of *CRLF2* (*ENSECAG00000037376*), which encodes a subunit of the TSLP receptor. This, together with prominent expression of *CD200R1*, argues for tolerogenic functions of equine tDC.

In further support of their involvement in inflammatory processes, equine tDC showed strong enrichment of *DPP4* and *IL17RA* transcripts, similar to porcine tDC (13). The peptidase CD26 (encoded by DPP4) is reported to regulate chemokine activity and thereby migration during inflammation (37), and with *IL17RA* transcripts, equine tDC appear well-equipped to respond to IL-17-rich environments, altogether suggesting their involvement in (bacterial) host defense, autoimmunity, and homeostasis of barrier tissues.

Expression of MHC-II-coding genes was lower in tDC than in cDC1 and cDC2, but considerably higher than in pDC, which is in line with transcriptomic studies performed in all three species investigated so far (12,13,18,36), and supporting their involvement in CD4 T-cell activation. Judging from the level of *WDFY4* detection, tDC may also be capable of cross-presentation. In addition, their expression of *FCGRT* (FcRn) suggests an enhanced ability to capture and present antigen-antibody immune complexes.

Moreover, equine tDC exhibited higher *CD5* expression than pDC and cDC2, mirroring observations in porcine, human and murine tDC (13,38). Notably, while CD5 may serve as a

358 conserved marker distinguishing tDC from cDC2 and pDC across species, its expression may
359 also indicate enhanced capabilities for T-cell priming (39).
360 Like porcine tDC, equine tDC were also strongly enriched in transcripts encoding Plexin 4A
361 (*PLXNA4*), a co-receptor for class 3 semaphorins. Notably, semaphorin 3A signaling was reported
362 to be important for DC transmigration into the lymphatic system by inducing actin-myosin
363 contraction (40). Although Plexin A1 was described as the involved co-receptor on DC in this
364 mouse study, Plexin A4 may serve a similar function in equine tDC for extravasating the vascular
365 or lymphatic system. It remains to be determined if and how tDC can enter lymph nodes to
366 engage in T-cell activation. We have preliminary data showing that porcine tDC upregulate CCR7
367 upon *in-vitro* TLR stimulation, which would suggest their migration to lymphatics via tissues.
368 Before similar experiments can be performed for equine tDC, a gating strategy will need to be
369 defined by flow cytometry. According to our transcriptomic and phenotypic data, it may be
370 sufficient to stain CD5, alongside Flt3, CD72a, CADM1, and CD14 on equine PBMC, although
371 their low frequency within DC may be challenging.
372 In our study, tDC were found to account for 4 % and 6 % of cells within DC for "Horse 1" and
373 "Horse 2", respectively, which is comparable to frequencies found in blood of humans and spleen
374 of mice (9,10,12,24,36,41), and contrasting with the high frequency (approx. 30 % detected within
375 DC) we recently reported in porcine blood (13). Future scRNA-seq studies should address
376 differences in frequency and gene expression of tDC across tissues and species and should
377 discuss possible implications for tDC biology. Tailored enrichment strategies will be necessary
378 for these comparisons to reduce gating bias in FACS, as discussed above.
379 Cross-species mapping of DC signatures by GSEA and cross-species integration confirmed our
380 annotation of equine DC subsets. Notably, our analyses suggest that cross-species integration
381 can be a powerful tool to refine cluster annotations, as indicated by the dispersed clustering of
382 murine pre-DC2 in the integrated dataset. Overall, robust cross-species comparisons of immune
383 cells should account as much as possible for factors affecting data comparability, most notably
384 hygienic/health status, tissue of origin and cell-enrichment strategies, among many other
385 factors. Regarding GSEA, we must note that gene signatures (obtained by DEA) are highly
386 dependent on the composition and clustering resolution of the initial dataset, with multiple sub-
387 clusters of a given subset likely leading to less powerful signatures, as may be the case for
388 signatures of murine and porcine tDC subsets used here.
389 Comparative analyses promise to considerably improve our understanding of newly described
390 DC subsets. The signatures obtained from the present study are a highly valuable resource,
391 paving the way for identifying and investigating DC subsets in lymphoid and non-lymphoid tissues

392 of horses. Ensuing studies should explore transcriptomic perturbations of these subsets in
393 equine immune-mediated pathologies and upon infection.

394 MATERIALS AND METHODS

395 Isolation of equine PBMC

396 Blood (100 mL) of three horses (Horse #1: male 10-year-old Freiberger; Horse #2: female 12-year-
397 old Freiberger; Horse #3: female 8-year-old Icelandic) was collected into vacutainer collection
398 tubes (Vacuette®; Greiner, St.Gallen, Switzerland) by puncturing the jugular vein, with sodium
399 heparin as anti-coagulant. Peripheral blood mononuclear cells (PBMC) were isolated by density
400 gradient centrifugation over Biocoll Separating Solution (density= 1.077 kg/l; Bioswisstec AG,
401 Schaffhausen, Switzerland). Erythrocytes were sedimented for 30 min at room temperature (RT)
402 before the upper leukocyte-rich plasma was collected and overlayed on Biocoll and then
403 centrifuged at 1,800 x g for 20 min (RT). The interphase layer with PBMC was transferred to a new
404 50 mL tube and washed twice with PBS, with a first centrifugation for 10 min at 290 x g and a
405 second centrifugation for 10 min at 200 x g (RT). Finally, PBMC were resuspended in PBS before
406 cell sorting. The study was approved by the Animal Experimental Committee of the Canton of
407 Bern, Switzerland (No. BE 2/17).

408 Phenotyping of equine PBMC and DC enrichment by FACS

409 Freshly isolated equine PBMC were stained in 96-well U-bottom plates with 10 x 10^6 cells per well
410 (phenotyping) or in 5 mL FACS tubes with 80 x 10^6 cells per tube (sorting experiments). Antibodies
411 against CD172a, CADM1, CD14, and CD163 (phenotyping only) were used, alongside
412 recombinant Flt3L. Bovine recombinant Flt3L-His, cross-reactive with equine Flt3, was produced
413 in house as previously described (4,42). All incubations were performed for 20 min at 4°C,
414 followed by washing with Cell Wash (BD Biosciences) and centrifugation at 500 x g for 5 min. Prior
415 to the staining, all samples were incubated with equine IgG (Biorad; PEP001; 50 µg/mL) to block
416 Fc receptors.
417 For phenotyping, cells were first incubated with anti-CD163 (LND68A; mIgG1) and anti-CADM1
418 (3E1; IgY), followed by incubation with matching secondary antibodies anti-mIgG1-PerCPeF710
419 (Invitrogen) and anti-IgY-biotin (Jackson ImmunoResearch). In the next step, ChromPure mouse-
420 IgG (Jackson ImmunoResearch) was added to block remaining binding sites of the anti-mIgG1
421 secondary antibody, alongside Streptavidin-BV421 (BD Horizon) and Flt3L-His. In the last step,
422 ZenonAF488-labeled anti-CD14 (105; mIgG1) was added alongside ZenonAF647-labeled anti-

423 CD172a (DH59B; mIgG1), anti-His-PE (mIgG1; Miltenyi Biotec GmbH), and LIVE/DEAD™ Fixable
424 Near-IR stain (Thermo Fisher Scientific). For enrichment of DC by FACS, PBMC were first
425 incubated with anti-CD172a (DH59B; mIgG1) and with anti-CADM1 (3E1; IgY), followed by
426 incubation with corresponding secondary antibodies anti-IgG1-A647 (Invitrogen, A-21240) and
427 anti-IgY-biotin (Jackson ImmunoResearch). Thereafter, cells were incubated with ChromPure
428 mouse-IgG (Jackson ImmunoResearch), Streptavidin-BV421 (BD Horizon) and Flt3L-His, and in a
429 final incubation step with ZenonAF488-labeled anti-CD14 (105; mIgG1), anti-His-PE (mIgG1;
430 Miltenyi Biotec GmbH), and LIVE/DEAD™ Fixable Near-IR stain (Thermo Fisher Scientific). Zenon
431 labeling kits were derived from Thermo Fisher Scientific. Samples were acquired with a
432 FACSCanto II flow cytometer (BD Biosciences) equipped with three lasers (405, 488, and 633
433 nm). Compensation was calculated by FACSDiva software using single-stained controls. Data
434 were analyzed using FlowJo software (v10.10, BD Biosciences). Sorting (FACS) was performed on
435 a MoFlo ASTRIOS EQ equipped with five lasers (355, 405, 488, 561, and 640 nm). A minimum of
436 30’000 cells was sorted. Cell counting and viability assessments were conducted on a TC20
437 automated cell counter (Biorad) using Trypan Blue dye 0.40 % (Biorad).

438 Single-cell RNA sequencing

439 Library preparation and sequencing were done at the Next Generation Sequencing (NGS)
440 Platform at the University of Bern. The three libraries were stored at minus 80°C, before being
441 pooled and sequenced in one run. GEM generation & barcoding, reverse transcription, cDNA
442 amplification and 3' gene expression library generation steps were all performed according to the
443 Chromium Single Cell 3' Reagent Kits v3 User Guide (10x Genomics CG000183 Rev B) with all
444 stipulated 10x Genomics reagents. Specifically, cell suspensions of between 700-1100 cells / µL
445 were prepared for the GEM generation and barcoding step with a targeted cell recovery of 5’000
446 cells. After the GEM-reverse transcription incubation, a clean-up step was performed followed by
447 12 cycles of cDNA amplification. The resulting cDNA was assessed for quantity and quality using
448 a Thermo Fisher Scientific Qubit 2.0 fluorometer with the Qubit dsDNA HS Assay Kit (Thermo
449 Fisher Scientific, Q32854) and an Advanced Analytical Fragment Analyzer System using a
450 Fragment Analyzer NGS Fragment Kit (Agilent, DNF-473), respectively. Thereafter, 3' gene
451 expression libraries were constructed using a sample index PCR step of 11 cycles. At the end of
452 the protocol, an additional 0.7x bead-based clean-up of the libraries was done. The produced
453 cDNA libraries were tested for quantity and quality using fluorometry and capillary
454 electrophoresis as defined above. The cDNA libraries were pooled and sequenced with a loading
455 concentration of 300 pM, paired end and single indexed, on an illumina NovaSeq 6000 sequencer

with a shared NovaSeq 6000 S2 Reagent Kit (100 cycles; illumina 20012862). The read set-up was as follows: read 1: 28 cycles, i7 index: 8 cycles, i5: 0 cycles and read 2: 91 cycles. The quality of the sequencing runs was assessed using illumina Sequencing Analysis Viewer (illumina version 2.4.7) and all base call files were demultiplexed and converted into FASTQ files using illumina bcl2fastq2 conversion software version 2.19.0. An average of 543'231'771 reads/library were obtained.

Analysis of equine scRNA-seq data

Genome reference and alignment

The raw sequencing data (FASTQ files) were processed using Cell Ranger v7.1 (10X Genomics) for read alignment to the equine reference genome, built with EquCab3.0 (INSDC Assembly GCA_002863925.1) as assembly and Ensembl EquCab3.0.111 as gene annotation. Filtered expression matrices from the three horses were generated using the "cellranger_count" pipeline with default arguments. Sample from "Horse 3" was excluded from further analysis (estimated number of cells: 179). Expression matrices were further analyzed in Python v3.9 (43) using scanpy v1.10.3 (44) and in R v4.3.3 (45) using mainly Seurat v5.3.0 (46), and other packages (complete list with references available on the GitHub page, see **Code availability** section).

Quality control and filtering

Scanpy v1.10.3 (44) was used for filtering the scRNA-seq data. Following single-cell best practices (47), we applied a median absolute deviation (MAD)-based outlier detection strategy with lenient thresholds across five quality control metrics. Accordingly, cells were excluded if they met any of the following criteria: (i) log-transformed total counts, (ii) log-transformed number of genes detected or (iii) percentage of total RNA counts from the 20 most highly expressed genes deviated more than 5 MADs above (> 5) or 3 MADs below (< 3) the median; (iv) percentage of mitochondrial gene counts > 10% or deviated beyond ± 5 MADs; and (v) percentage of hemoglobin gene counts > 5% or deviated < 8 or > 3 MADs. Thus, each sample was individually filtered and then processed for removal of doublets using scrublet v0.2.3 (48).

Data integration, dimensionality reduction and clustering

We applied scVI (Single-cell Variational Inference) (49) to integrate and batch-correct the data, with sample origin as a covariate. Default parameters were used, except for "n_latent = 30" and "n_layers = 2". The scVI latent space was used for non-linear dimensionality reduction using UMAP and to construct the neighborhood graph for Leiden clustering at different resolutions.

487 **Differential gene expression analysis (DEA)**

488 We used Seurat v5.3.0 (46) for DEA on normalized and log-transformed data. The differentially
489 expressed genes (DEGs) in each cluster were identified with the *FindAllMarkers()* function and
490 pairwise comparisons between selected clusters were performed with the *FindMarkers()*
491 function. Only genes expressed in at least 20% of the cells in one of the clusters being compared,
492 and with adjusted p-value < 0.05, were selected as DEGs. For pairwise comparisons, DEGs found
493 in 100% of the cells from both compared groups (pct.1 = 1 and pct.2 = 1) were filtered out.
494 Complete gene lists from DEA are given in **Supplementary Table 1-3.**

495 **Gene module scoring**

496 Average expression levels of gene sets (module scores) in each cell were estimated using Seurat's
497 *AddModuleScore()* function. The MHC-II module scores were calculated based on seven MHC-II-
498 coding genes (*HLA-DRA*, *HLA-DOA*, *HLA-DOB*, *HLA-DMA*, *HLA-DMB*, *ELA-DRB* and *ELA-DQB*)
499 using "ctrl = 25" and "nbin = 15" to ensure stable expression binning and control gene selection
500 in the equine dataset. Inflammatory response (166 genes) and complement (164 genes) modules
501 were defined from the Hallmark gene sets of the human Molecular Signature Database (MSigDB)
502 using msigdbr v25.1.1 (50). Human genes were mapped to equine orthologs using BioMart
503 (Ensembl; https://www.ensembl.org/biomart/martview), retaining only one-to-one orthologous
504 pairs, and module scores were computed with "ctrl = 50" and "nbin = 24".

505 **Pathway and transcription factor activity inference**

506 The PROGENy and CollecTRI databases (human) were used to infer pathway and transcription
507 factor activities, respectively, in the two equine cDC2 single-cell clusters (c0 and c3) with
508 decoupleR v2.8.0 (51). Regulatory activity scores were estimated using the *run_mlm()* function,
509 which applied a multivariate linear model to normalized log-transformed counts. Following score
510 scaling, differentially regulated transcription factors (TFs) were identified with the
511 *FindAllMarkers()* function. Only TFs with |avg_log2FC| > 1 and adjusted p-value < 0.05 were
512 considered as differentially regulated. Complete resulting TF list is given in **Supplementary Table**
513 **3.**

514 **Gene ontology over-representation analysis (ORA)**

515 Enriched gene ontology (GO) Biological Process (BP) terms for cDC2A (c0) and cDC2B (c3) were
516 identified using the *compareCluster()* function (fun = "enrichGO", ont = "BP", OrgDb =
517 org.Hs.eg.db) from the clusterProfiler v4.10.1 package (52). Equine cluster-specific gene
518 signatures previously defined by DEA (see **Supplementary Table 1-3**) were first mapped to their

519 human orthologs (ENTREZ ID format) using BioMart (Ensembl). To retain the most biologically
520 informative categories, only enriched GO BP terms corresponding to levels 4-7 in the GO
521 hierarchy (based on ancestor counts) were included.

522 **Integration with public equine dataset (PBMC-derived DC and monocytes)**

523 Our equine scRNA-seq dataset of enriched DC (5581 cells) was integrated with DC and
524 monocytes subsetted from a published equine PBMC dataset (2981 cells) (16). First, the PBMC
525 data was re-processed from the publicly available count matrices generated using End Sequence
526 Analysis Toolkit (ESAT) (53) (see **Data Availability**, and **Code Availability** for detailed pipeline).
527 According to the initial analysis performed by Patel *et al.*, monocyte and DC clusters were
528 selected and subclusters were characterized, allowing the identification of the main DC and
529 monocyte subsets (**Supp. Fig. 4A-B**). A small cluster of low-quality cells (low number of genes
530 and transcripts, high percentage of mitochondrial gene expression), as well as a cluster showing
531 a strong neutrophil signature, were excluded from further analyses. Next, our dataset was re-
532 processed using Ensembl v95 and ESAT (53) following the procedures originally described by the
533 authors (16), to allow direct comparison with their dataset. After re-analysis, all previously
534 identified DC subsets (**Fig. 1B**) were recovered based on marker gene expression profiles (**Supp.
535 Fig. 4C**). A minor group of low-quality cells was filtered out prior to downstream analyses. Finally,
536 both datasets were integrated as follows: (i) Each of the 9 samples (7 horses from Patel *et al.* and
537 2 horses from in-house dataset) were independently processed for sctransform-based
538 normalization; (ii) Linear dimensionality reduction using PCA was performed, followed by data
539 integration with Harmony v1.2.4 (54) selecting the sample as a covariate; (iii) Harmony
540 embeddings were used for identifying nearest neighbors, Leiden clustering (method = "igraph",
541 resolution = 0.6), and non-linear dimensionality reduction using UMAP for cluster visualization in
542 the integrated dataset (**Supp. Fig. 4D**).

543 **Cross-species gene set enrichment analysis (GSEA)**

544 Gene set enrichment analyses were performed with the AUCell package v1.24.0 (55) as initially
545 described by Herrera-Uribe *et al.* (56) and recently adapted by Baillou et *al.* (13). The enrichment
546 of DC subset gene signatures from various species were evaluated in the equine scRNA-seq
547 dataset by calculating area under the curve (AUC) scores, which represent the proportion of
548 genes from each signature that are included among the top 25% expressed genes in each cell.
549 For each gene set, thresholds were determined manually based on AUC score distributions.
550 (**Supp. Fig. 5**). The DC subset gene signatures were selected from four sources: (i) our recently
551 published scRNA-seq study of porcine blood DC (10x Genomics) (13), (ii) a cDC2-focused review

552 integrating five public murine DC scRNA-seq datasets (29), (ii) a published bulk and scRNA-seq
553 study of murine spleen DC (10x Genomics) (12), and (iii) a published scRNA-seq dataset (10x
554 Genomics) of human blood DC (50) that we previously re-analyzed (13). Equine one-to-one
555 orthologs of pig, human and mouse genes were identified with BioMart (Ensembl) and selected
556 based on the highest percentage identity to the target equine gene. Genes lacking an equine
557 ortholog were excluded. The resulting horse-converted pig, human and murine gene signatures
558 are provided in **Supplementary Table 4**.

559 **Single-cell data integration across species using Harmony**

560 Our equine scRNA-seq dataset (5581 cells) was integrated with three public datasets, including
561 scRNA-seq data of blood DC population from pig (33922 cells) (13), human (2979 cells) (36) and
562 mouse (6738 cells) (11), using Seurat v5.3.0 (46). The original porcine dataset was randomly down
563 sampled to 10,000 cells and monocyte clusters were removed from the original murine dataset.
564 First, human orthologs of the genes comprised in the equine, porcine and murine datasets were
565 identified with BioMart (Ensembl). All datasets were then subsetted to their shared common
566 genes (11,402 genes) and merged. Samples were independently processed for sctransform-
567 based normalization (1 layer/individual or 1 layer/dataset according to the information available
568 from each dataset), including steps of data scaling and highly variable gene identification, and for
569 linear dimensionality reduction using PCA. For further downstream analysis, the optimal number
570 of 30 principal components was identified by the elbow plot method. Next, data integration of the
571 four datasets was performed with Harmony v1.2.4 (54) on PCA cell embeddings and selecting the
572 sample origin (either individual or dataset level) and the species as covariates (batch effect
573 correction). The resulting Harmony reduction was selected for identifying nearest neighbors,
574 Leiden clustering (method = “igraph”, resolution = 0.4), and non-linear dimensionality reduction
575 using UMAP for data visualization.

576 **Cluster correlation analysis**

577 Cluster correlation analysis was performed using Seurat’s *BuildClusterTree()* function on the
578 Harmony-corrected embeddings (dims = 1:30). Euclidean distances were computed between
579 cluster centroids, followed by hierarchical clustering (method = "average"). The resulting
580 similarity tree was visualized using the ape v5.8-1 R package (57).

581 Identification and replacement of gene identifiers

582 Horse gene Ensembl stable identifiers (IDs) without available gene name/symbol in the equine
583 genome annotation file were replaced in text and figures by NCBI gene (formerly Entrezgene)

accession or UniProtKB Gene Name symbol if available in the corresponding databases using BioMart (Ensembl). For genes lacking direct annotation, human orthologs were identified either through Ensembl ortholog mapping or by sequence similarity using BLAST against the human genome (GRCh38.p14). Replaced Ensembl IDs are listed in **Supplementary Table 1**. The human gene names *HLA-DOA*, *HLA-DOB*, *HLA-DMA*, *HLA-DMB* and *HLA-DRA* found in the equine genome annotation were replaced by the gene names of their equine orthologs, i.e. *ELA-DOA*, *ELA-DOB*, *ELA-DMA*, *ELA-DMB* and *ELA-DRA*, respectively.

Preparation of Figures

Figures were prepared using FlowJo™ v10.10.0 (BD Life Sciences), R v4.3.3 (45), Rstudio v2025.09.0 (58), and Adobe Illustrator v30.2.1 (https://adobe.com/products/illustrator) and Inkscape v1.3.2 (https://www.inkscape.org) softwares.

Visualization of scRNA-seq data was based on feature plots, dot plots, violin plots, scatter plots, heatmaps and histograms using Seurat v5.3.0 (46), scCustomize v3.2.0 (59), ggplot2 v3.5.2 (60), ComplexHeatmap v2.18.0 (61) and AUCell v1.24.0 (55) R packages. Heatmaps were generated with scaled and centered data (Seurat *ScaleData()* function). For improved contrast in feature plots, feature-specific contrast levels were calculated based on quantiles (q10, q90) of non-zero expression.

DATA AVAILABILITY

Raw sequencing data from scRNA-seq of equine blood-enriched DC will be available in the European Nucleotide Archive (ENA) upon publication of the final version. Processed scRNA-seq data are available from the corresponding author upon request.

Public scRNA-seq datasets used in this study included: (i) Equine PBMC (16), available in the NCBI GEO database under the accession number GSE148416; (ii) Porcine blood DC (13), available in ENA under the accession number PRJEB101131; (iii) Murine blood DC (11), downloaded from https://doi.org/10.6084/m9.figshare.22232056.v1; and (iv) Human blood DC (36), available in the NCBI GEO database under the accession number GSE276518.

CODE AVAILABILITY

Code and packages used for scRNA-seq data analyses will be available in a GitHub public repository upon publication of the final version.

AUTHOR CONTRIBUTIONS

Ambre Baillou (Formal analysis, Methodology, Visualization, Writing – original draft), Marius Botos (Formal analysis, Visualization, Writing – review & editing), Simone Oberhaensli (Formal analysis, Writing – review & editing), Iva Cvitas (Data curation, Writing – review & editing), Sigridur Jonsdottir (Data curation, Writing – review & editing), Anja Ziegler (Formal analysis, Writing – review & editing), Francisco Brito (Formal analysis, Writing – review & editing), Artur Summerfield (Conceptualization, Resources, Writing – review & editing), Eliane Marti (Conceptualization, Resources, Writing – review & editing), Stephanie C. Talker (Conceptualization, Methodology, Supervision, Formal Analysis, Visualization, Writing – original Draft).

ACKNOWLEDGEMENTS

We thank Roosheel Patel and Brad Rosenberg (Department of Microbiology, Icahn School of Medicine at Mount Sinai, USA) for ESAT processing of our dataset. Moreover, we thank Stefan Müller (FCCS, University of Bern, Switzerland) for cell sorting, the team of the NGS platform (NGSP, University of Bern, Switzerland) for single-cell RNA sequencing, and the Interfaculty Bioinformatics Unit (IBU, University of Bern, Switzerland) for access to their compute cluster.

CONFLICT OF INTEREST

The authors declare that the research was conducted in the absence of any commercial or financial relationships that could be construed as a potential conflict of interest.

633 # FIGURE LEGENDS

634 **Figure 1: Identification of main DC subsets in equine blood by scRNA-seq.** (**A**) Gating
635 strategy to enrich DC from equine PBMC for scRNA-seq by FACS (large
636 cells/singlets/alive/Flt3^{+}CADM1$^{+/hi}$). (**B**) UMAP plot with annotation of putative DC progenitors,
637 cDC1, cDC2-like cells, and pDC. (**C**) Feature plots of key markers used for subset identification.
638 (**D**) Dot plot with additional DC subset-specific genes. (**E**) Heatmap with top 15 differentially
639 expressed genes. Complete gene lists are given in **Supp. Table 1**. (**F**) Violin plots show transcript
640 expression for phenotypic markers previously analyzed by flow cytometry.
641
642 **Figure 2: Delineation of tDC and putative DC3 from cDC2.** (**A**) Annotation of cDC2-like clusters
643 in UMAP plot. (**B**) Feature plots show expression of CD1 genes, enriched in cDC2. (**C**) Feature
644 plots show expression of pDC-related genes, enriched in tDC. (**D**) Feature plots show expression
645 of pro-inflammatory genes (*FCN1*, *S100A12*, *C5AR1*), enriched in DC3 (c5). **(E)** Scatter plots show
646 co-expression of *FLT3* and monocyte markers (*CSF1R*, *CD163*) at the single-cell level in cluster 5
647 (DC3). (**F**) Feature plots of cDC2-like cells showing module scores for the Hallmark gene sets
648 "inflammatory response" and "complement". (**G**) Feature plot of cDC2-like cells showing MHC-II
649 score (custom gene module, see **M&M**). (**H**) Heatmaps showing top 20 DEGs from pairwise
650 comparisons between cDC2 (c0&c3) and tDC on the left, and between cDC2 (c0&c3) and DC3
651 on the right. Complete gene lists are given in **Supp. Table 2**.
652
653 **Figure 3: Heterogeneity of cDC2.** (**A**) Annotation of cDC2 subsets (cDC1.1, cDC2.2) in UMAP
654 plot and their expression of *FCER1A* and CX3CR1 visualized in feature plots. (**B**) Heatmap
655 displays top 20 differentially expressed genes (DEGs) between cDC2 subsets. Complete gene
656 lists are given in **Supp. Table 3**. (**C**) Violin plots show selected DEGs between cDC2 subsets. (**D**)
657 Feature plots show inferred regulatory activity scores for selected PROGENy pathways across the
658 two cDC2 clusters. (**E**) Dot plot illustrates selected enriched Gene Ontology (GO) biological
659 process terms in the two cDC2 clusters, as determined by over-representation analysis. (**F**)
660 Feature plots show inferred regulatory activity scores for selected differentially regulated
661 transcription factors (TF) across the two cDC2 clusters. Complete TF list is given in **Supp. Table**
662 **3.**
663
664
665
666

667 **Figure 4: Challenges in delineating DC from monocytes.** (**A**) Our in-house dataset (enriched
668 equine DC) was re-processed according to Patel *et al.* and integrated with DC and monocytes
669 from this previously published dataset (Patel *et al.*, equine PBMC). (**B**) UMAP plot shows
670 annotation of ten clusters in integrated dataset. (**C**) UMAP plots show location of initial clusters
671 (depicted in **Fig. 4A**) on integrated dataset. (**D**) Bar plots show contributions (cell proportions) of
672 initial datasets (in-house vs. Patel *et al.*) to clusters in integrated dataset. (**E**) Key marker genes
673 visualized in feature plots on the integrated UMAP, split by dataset (in-house vs. Patel *et al.*). (**F**)
674 Key marker genes visualized as violin plots for clusters in integrated dataset. Clusters 4 and 3
675 were highlighted by dashed frames. (**G**) Scatter plots illustrate co-expression of *FLT3* and *LYZ* or
676 *CD163* in cells of cluster 4 (blue) and cluster 3 (green) by dataset (in-house vs. Patel *et al.*).
677

678 **Figure 5: Gene expression related to main DC functions.** (**A**) Cluster annotation. (**B-H**) Dot
679 plots visualize gene expression across all annotated clusters related to pattern recognition (**B**),
680 antigen presentation and T-cell modulation (**C**), cytokines and receptors (**D**), migration (**E**),
681 adhesion (**F**), Fc receptors (**G**) and complement (**H**).

682

683 **Figure 6: Cross-species comparison of DC subsets.** (**A**) UMAP plot showing cluster annotation
684 for equine DC subsets. (**B-D**) Heatmaps showing averaged scaled enrichment scores for gene
685 signatures from porcine blood DC subsets (Baillou *et al.*), from murine splenic DC (Sulczewski *et*
686 *al.*), and from human blood DC (Lubin *et al.*, re-analyzed by Baillou *et al.*), calculated using the
687 AUC method (see **Supp. Table 4** for gene signatures). AUC relative scores >= 0.5 are displayed.
688 (**E**) Integration of scRNA-seq datasets of blood-enriched DC from horse, pig (Baillou *et al.*),
689 human (Lubin *et al.*, re-analyzed by Baillou *et al.*) and mouse (Liu *et al.*). UMAP plots show initial
690 datasets and their respective cluster annotations. (**F**) UMAP plot showing cluster annotation for
691 cross-species integrated dataset. (**G**) UMAP plots showing location of initial clusters (depicted in
692 **Fig. 6E**) on integrated dataset. (**H**) Similarity tree showing correlations between the initial species-
693 specific clusters in the integrated dataset, calculated using Euclidean distances.
694
695
696
697
698

699 **Supplementary Figure 1: Phenotyping and enrichment of equine DC.** (**A**) Phenotyping of
700 putative DC and monocyte subsets. Within the Flt3 gate, putative DC and monocyte subsets were
701 defined based on expression of CD14 and CADM1. Localization of subsets in overlayed dot plot
702 showing CD172a vs. Flt3. For each subset, expression levels of CD163 and CD172a were
703 visualized in histograms, alongside FSC-A signal intensity. (**B**) Original gates used to enrich DC for
704 scRNA-seq.
705
706 **Supplementary Figure 2: Quality control and cluster proportions.** (**A**) Retained cells in horses
707 #1-3 following QC filtering. For each horse, stacked bar plots show the number of cells retained
708 in the analysis (green), the number of cells removed due to low quality (purple; low number of
709 reads, low number of genes, high proportion of total RNA counts that come from the 20 most
710 highly expressed genes, high percentage of mitochondrial reads, high percentage of hemoglobin
711 reads), and the number of cells detected as doublets and removed (orange). (**B**) Cluster
712 annotation and proportions of cell types found in Horse #1 and Horse #2.
713
714 **Supplementary Figure 3**: **Enrichment of murine cDC2A and cDC2B signatures in equine**
715 **cDC2.** Cross-species gene set enrichment analysis of equine cDC2 (c0&c3) using gene
716 signatures of murine cDC2A and cDC2B derived from integrated murine blood, spleen and bone-
717 marrow datasets (Baber *et al.*). Histograms show the distributions of enrichment scores.
718 Threshold values (vertical red lines) were manually determined for each gene signature to
719 distinguish non-enriched from enriched cells for visualization in feature plots. Enrichment levels
720 among enriched cells (values > threshold) were visualized using a gradient color scale ranging
721 from low (blue) to high (yellow) in feature plots. Heatmap visualizes enrichment scores across the
722 two equine cDC2 clusters. Averaged, scaled AUC relative score with value >= 0.5 displayed in
723 heatmap.
724
725 **Supplementary Figure 4: Integration of in-house and published equine datasets for**
726 **delineation of DC from monocytes.** (**A**) The equine PBMC single-cell dataset from Patel *et al.*
727 was used to subset monocytes and dendritic cells (DC). UMAP plot shows annotation of the main
728 cell types (T cells, B cells, basophils, monocytes/DC), identified by their specific marker
729 expression visualized in feature plots. (**B**) Monocytes and DC were selected from the PBMC
730 dataset of Patel *et al.*, and cell subsets were identified based on key marker expression visualized
731 in feature plots. Violin plots show quality metrics (number of genes and transcripts, percentage
732 of mitochondrial gene expression) across clusters for identifying low-quality cells. One monocyte

733 cluster appeared to contain neutrophils, judging from its lower gene and transcript content and
734 specific expression of the key markers *CSF3R*, *S100A8*, *S100A9*, *E-CATH3*, and was thus removed
735 prior to integration. (**C**) Our in-house dataset (enriched equine DC) was re-processed according
736 to Patel *et al.*, and the previously identified DC subsets (**Fig. 1B**) were recovered based on key
737 marker expression (shown in feature plots). Violin plots show quality metrics (number of genes
738 and transcripts, percentage of mitochondrial gene expression) across clusters for identifying low-
739 quality cells. (**D**) Our in-house DC dataset (excluding low-quality cells) and the monocyte/DC
740 dataset from Patel *et al.* (excluding low-quality cells and putative neutrophils) were integrated.
741 UMAP plot displays the annotated cell subsets in the integrated dataset, based on key marker
742 expression visualized in feature plots.
743
744 **Supplementary Figure 5: Cross-species DC signature enrichment**. Gene signatures from
745 porcine blood DC subsets (Baillou *et al.*; **A**), murine spleen DC (Sulczewski *et al.*; **B**) and human
746 blood DC (Lubin *et al.*, re-analyzed by Baillou *et al.*; **C**) were used for gene set enrichment analysis
747 of the equine scRNA-seq dataset. Histograms show the distribution of enrichment scores.
748 Threshold values (vertical red lines) were manually determined for each gene signature to
749 distinguish non-enriched from enriched cells for visualization in feature plots. Enrichment levels
750 among enriched cells (values > threshold) were visualized using a gradient color scale ranging
751 from low (blue) to high (yellow). See **Code Availability** for more details. For visualization of
752 enrichment scores in heatmaps refer to **Fig. 6B-D**.
753
754 **Supplementary Figure 6: Cross-species DC integration**. Integration of scRNA-seq datasets of
755 blood-enriched DC from horse, pig (Baillou *et al.*), human (Lubin *et al.*, re-analyzed by Baillou *et*
756 *al.*) and mouse (Liu *et al.*) (related to **Fig. 6E-H**). (**A**) UMAP plot showing subset annotation for
757 integrated dataset and pie charts displaying the percentage of DC subsets from each species
758 contributing to clusters 1, 3, and 5 of the integrated dataset, normalized to their respective initial
759 dataset sizes. (**B**) Feature plots by species showing expression of key marker genes for DC
760 subsets in integrated dataset.
761

REFERENCES

1. Eisenbarth SC. Dendritic cell subsets in T cell programming: location dictates function. Nat Rev Immunol. 2019 Feb;19(2):89–103. doi:10.1038/s41577-018-0088-1

2. Collin M, Bigley V. Human dendritic cell subsets: an update. Immunology. 2018 May;154(1):3–20. doi:10.1111/imm.12888

3. Reizis B. Plasmacytoid Dendritic Cells: Development, Regulation, and Function. Immunity. 2019 Jan 15;50(1):37–50. doi:10.1016/j.immuni.2018.12.027

4. Ziegler A, Marti E, Summerfield A, Baumann A. Identification and characterization of equine blood plasmacytoid dendritic cells. Dev Comp Immunol. 2016 Dec;65:352–7. doi:10.1016/j.dci.2016.08.005 PubMed PMID: 27524460.

5. Summerfield A, Auray G, Ricklin M. Comparative dendritic cell biology of veterinary mammals. Annual review of animal biosciences. 2015;3:533–57. doi:10.1146/annurev-animal-022114-111009

6. Entrican G, Lunney JK, Wattegedera SR, Mwangi W, Hope JC, Hammond JA. The Veterinary Immunological Toolbox: Past, Present, and Future. Front Immunol. 2020 Jul 28;11. doi:10.3389/fimmu.2020.01651

7. Bourdely P, Anselmi G, Vaivode K, Ramos RN, Missolo-Koussou Y, Hidalgo S, et al. Transcriptional and Functional Analysis of CD1c+ Human Dendritic Cells Identifies a CD163+ Subset Priming CD8+CD103+ T Cells. Immunity. 2020 Aug;53(2):335-352.e8. doi:10.1016/j.immuni.2020.06.002

8. Villar J, Segura E. The More, the Merrier: DC3s Join the Human Dendritic Cell Family. Immunity. 2020 Aug;53(2):233–5. doi:10.1016/j.immuni.2020.07.014

9. Villani AC, Satija R, Reynolds G, Sarkizova S, Shekhar K, Fletcher J, et al. Single-cell RNA-seq reveals new types of human blood dendritic cells, monocytes, and progenitors. Science. 2017 Apr 21;356(6335):eaah4573. doi:10.1126/science.aah4573

10. Leylek R, Alcántara-Hernández M, Lanzar Z, Lüdtke A, Perez OA, Reizis B, et al. Integrated Cross-Species Analysis Identifies a Conserved Transitional Dendritic Cell Population. Cell Reports. 2019 Dec;29(11):3736-3750.e8. doi:10.1016/j.celrep.2019.11.042

11. Liu Z, Wang H, Li Z, Dress RJ, Zhu Y, Zhang S, et al. Dendritic cell type 3 arises from Ly6C+ monocyte-dendritic cell progenitors. Immunity. 2023 Aug 8;56(8):1761-1777.e6. doi:10.1016/j.immuni.2023.07.001

12. Sulczewski FB, Maqueda-Alfaro RA, Alcántara-Hernández M, Perez OA, Saravanan S, Yun TJ, et al. Transitional dendritic cells are distinct from conventional DC2 precursors and mediate proinflammatory antiviral responses. Nat Immunol. 2023 Aug;24(8):1265–80. doi:10.1038/s41590-023-01545-7

13. Baillou A, Auray G, Brito F, Botos M, Huber A, Summerfield A, et al. Unraveling porcine dendritic-cell diversity: welcome tDC and DC3. Front Immunol. 2025 Oct 29;16:1639553. doi:10.3389/fimmu.2025.1639553

14. Amon L, Seichter A, Vurnek D, Heger L, Lächele L, Tochoedo NR, et al. Clec12A, CD301b, and FcγRIIB/III define the heterogeneity of murine DC2s and DC3s. Cell Reports. 2024 Mar;43(3):113949. doi:10.1016/j.celrep.2024.113949

15. Cytlak U, Resteu A, Pagan S, Green K, Milne P, Maisuria S, et al. Differential IRF8 Transcription Factor Requirement Defines Two Pathways of Dendritic Cell Development in Humans. Immunity. 2020 Aug 18;53(2):353-370.e8. doi:10.1016/j.immuni.2020.07.003 PubMed PMID: 32735845; PubMed Central PMCID: PMC7447982.

16. Patel RS, Tomlinson JE, Divers TJ, Van De Walle GR, Rosenberg BR. Single-cell resolution landscape of equine peripheral blood mononuclear cells reveals diverse cell types including T-bet+ B cells. BMC Biol. 2021 Dec;19(1):13. doi:10.1186/s12915-020-00947-5

17. Guivarch M, Meyer P, Braud A, Marschall P, Perrin A, Verdenet A, et al. TSLP promotes GATA3-expressing effector regulatory T cells via DC2 derived from transitional DCs. Nat Immunol. 2026 Feb;27(2):348–63. doi:10.1038/s41590-025-02400-7

18. Valente M, Collinet N, Vu Manh TP, Popoff D, Rahmani K, Naciri K, et al. Novel mouse models based on intersectional genetics to identify and characterize plasmacytoid dendritic cells. Nat Immunol. 2023 Apr;24(4):714–28. doi:10.1038/s41590-023-01454-9

19. Sage SE, Leeb T, Jagannathan V, Gerber V. Single-cell profiling of bronchoalveolar cells reveals a TH17 signature in neutrophilic severe equine asthma. Immunology. 2024 Apr;171(4):549–65. doi:10.1111/imm.13745

20. Sage SE, Nicholson P, Peters LM, Leeb T, Jagannathan V, Gerber V. Single-cell gene expression analysis of cryopreserved equine bronchoalveolar cells. Front Immunol. 2022 Aug 23;13:929922. doi:10.3389/fimmu.2022.929922

21. Riihimäki M, Fegraeus K, Nordlund J, Waern I, Wernersson S, Akula S, et al. Single-cell transcriptomics delineates the immune cell landscape in equine lower airways and reveals upregulation of FKBP5 in horses with asthma. Sci Rep. 2023 Sep 27;13(1):16261. doi:10.1038/s41598-023-43368-4

22. Ammons DT, Chow L, Goodrich L, Bass L, Larson B, Williams ZJ, et al. Characterization of the single cell landscape in normal and osteoarthritic equine joints. Ann Transl Med. 2024 Oct;12(5):88–88. doi:10.21037/atm-24-40

23. Jaworska J, Tobolski D, Salem SE, Kahler A, Wocławek-Potocka I, De Mestre AM. Single-cell atlas of the pregnant equine endometrium before and after implantation. Biology of Reproduction. 2025 Mar 16;112(3):458–73. doi:10.1093/biolre/ioaf004

24. Rodrigues PF, Trsan T, Cvijetic G, Khantakova D, Panda SK, Liu Z, et al. Progenitors of distinct lineages shape the diversity of mature type 2 conventional dendritic cells. Immunity. 2024 Jul 9;57(7):1567-1585.e5. doi:10.1016/j.immuni.2024.05.007

25. Brown CC, Gudjonson H, Pritykin Y, Deep D, Lavallée VP, Mendoza A, et al. Transcriptional Basis of Mouse and Human Dendritic Cell Heterogeneity. Cell. 2019 Oct;179(4):846-863.e24. doi:10.1016/j.cell.2019.09.035

26. Buggins AGS, Mufti GJ, Salisbury J, Codd J, Westwood N, Arno M, et al. Peripheral blood but not tissue dendritic cells express CD52 and are depleted by treatment with alemtuzumab. Blood. 2002 Sep 1;100(5):1715–20. doi:10.1182/blood.V100.5.1715.h81702001715_1715_1720

27. Rodriguez-Manzanet R, Meyers JH, Balasubramanian S, Slavik J, Kassam N, Dardalhon V, et al. TIM-4 Expressed on APCs Induces T Cell Expansion and Survival. The Journal of Immunology. 2008 Apr 1;180(7):4706–13. doi:10.4049/jimmunol.180.7.4706

28. Talker SC, Hope JC, Summerfield A. Phenotype of bovine mononuclear phagocytes– An update. Veterinary Immunology and Immunopathology. 2024 Nov;277:110836. doi:10.1016/j.vetimm.2024.110836

29. Baber RW, Magalhães-Patrício MÂ, Pires MV, Correia V, Lozano-Gil JM, Guimarães JC, et al. Ontogenetic Diversification of Type 2 Conventional Dendritic Cells in the Bone Marrow: A Central Logic for Peripheral Immunity. Immunological Reviews. 2025 Nov;336(1):e70077. doi:10.1111/imr.70077

30. Minutti CM, Piot C, Pereira da Costa M, Chakravarty P, Rogers N, Huerga Encabo H, et al. Distinct ontogenetic lineages dictate cDC2 heterogeneity. Nat Immunol. 2024 Mar;25(3):448–61. doi:10.1038/s41590-024-01745-9

31. León B. Type 2 conventional dendritic cell functional heterogeneity: ontogenically committed or environmentally plastic? Trends in Immunology. 2025 Feb;46(2):104–20. doi:10.1016/j.it.2024.12.005

32. Tussiwand R, Rodrigues PF. Where's Waldo: Identifying DCs within Mononuclear Phagocytes during Inflammation. Immunity. 2020 Jun 16;52(6):892–4. doi:10.1016/j.immuni.2020.05.006

33. Dutertre CA, Becht E, Irac SE, Khalilnezhad A, Narang V, Khalilnezhad S, et al. Single-Cell Analysis of Human Mononuclear Phagocytes Reveals Subset-Defining Markers and Identifies Circulating Inflammatory Dendritic Cells. Immunity. 2019 Sep 17;51(3):573-589.e8. doi:10.1016/j.immuni.2019.08.008

34. Auray G, Keller I, Python S, Gerber M, Bruggmann R, Ruggli N, et al. Characterization and Transcriptomic Analysis of Porcine Blood Conventional and Plasmacytoid Dendritic Cells Reveals Striking Species-Specific Differences. The Journal of Immunology. 2016 Dec 15;197(12):4791–806. doi:10.4049/jimmunol.1600672

35. Talker SC, Baumann A, Bruggmann R. Precise Delineation and Transcriptional Characterization of Bovine Blood Dendritic-Cell and Monocyte Subsets. Front Immunol. 2018 Oct 30;9. doi:10.3389/fimmu.2018.02505

36. Lubin R, Patel AA, Mackerodt J, Zhang Y, Gvili R, Mulder K, et al. The lifespan and kinetics of human dendritic cell subsets and their precursors in health and inflammation. Journal of Experimental Medicine. 2024 Nov 4;221(11):e20220867. doi:10.1084/jem.20220867

37. Metzemaekers M, Van Damme J, Mortier A, Proost P. Regulation of Chemokine Activity - A Focus on the Role of Dipeptidyl Peptidase IV/CD26. Front Immunol. 2016;7:483. doi:10.3389/fimmu.2016.00483 PubMed PMID: 27891127; PubMed Central PMCID: PMC5104965.

38. Idoyaga J, Ni H, Maqueda-Alfaro RA. Bridging pDCs and cDCs : The Identity of Transitional Dendritic Cells. Immunological Reviews. 2025 Nov;336(1):e70070. doi:10.1111/imr.70070

39. He M, Roussak K, Ma F, Borcherding N, Garin V, White M, et al. CD5 expression by dendritic cells directs T cell immunity and sustains immunotherapy responses. Science. 2023 Feb 17;379(6633):eabg2752. doi:10.1126/science.abg2752

40. Takamatsu H, Takegahara N, Nakagawa Y, Tomura M, Taniguchi M, Friedel RH, et al. Semaphorins guide the entry of dendritic cells into the lymphatics by activating myosin II. Nat Immunol. 2010 Jul;11(7):594–600. doi:10.1038/ni.1885 PubMed PMID: 20512151; PubMed Central PMCID: PMC3045806.

41. Alcántara-Hernández M, Leylek R, Wagar LE, Engleman EG, Keler T, Marinkovich MP, et al. High-Dimensional Phenotypic Mapping of Human Dendritic Cells Reveals Interindividual Variation and Tissue Specialization. Immunity. 2017 Dec;47(6):1037-1050.e6. doi:10.1016/j.immuni.2017.11.001

42. Guzylack-Piriou L, Alves MP, McCullough KC, Summerfield A. Porcine Flt3 ligand and its receptor: generation of dendritic cells and identification of a new marker for porcine dendritic cells. Developmental and comparative immunology. 2010 Apr;34(4):455–64. doi:10.1016/j.dci.2009.12.006

43. Python Software Foundation. Python Language Reference, version 3.9 [Internet]. 2020. Available from: https://docs.python.org/3.9/

44. Wolf FA, Angerer P, Theis FJ. SCANPY: large-scale single-cell gene expression data analysis. Genome Biology. 2018 Feb 6;19(1):15. doi:10.1186/s13059-017-1382-0

45. R Core Team. R: A Language and Environment for Statistical Computing [Internet]. Vienna, Austria: R Foundation for Statistical Computing; 2023. Available from: https://www.R-project.org/

46. Hao Y, Stuart T, Kowalski MH, Choudhary S, Hoffman P, Hartman A, et al. Dictionary learning for integrative, multimodal and scalable single-cell analysis. Nat Biotechnol. 2023 May 25. doi:10.1038/s41587-023-01767-y

47. Heumos L, Schaar AC, Lance C, Litinetskaya A, Drost F, Zappia L, et al. Best practices for single-cell analysis across modalities. Nat Rev Genet. 2023 Aug;24(8):8. doi:10.1038/s41576-023-00586-w

48. Wolock SL, Lopez R, Klein AM. Scrublet: Computational Identification of Cell Doublets in Single-Cell Transcriptomic Data. Cell Systems. 2019 Apr 24;8(4):281-291.e9. doi:10.1016/j.cels.2018.11.005

49. Lopez R, Regier J, Cole MB, Jordan MI, Yosef N. Deep generative modeling for single-cell transcriptomics. Nat Methods. 2018 Dec;15(12):12. doi:10.1038/s41592-018-0229-2

50. Dolgalev I. msigdbr: MSigDB Gene Sets for Multiple Organisms in a Tidy Data Format [Internet]. 2018 [cited 2025 Dec 12]. p. 25.1.1. Available from: https://CRAN.R-project.org/package=msigdbr doi:10.32614/CRAN.package.msigdbr

51. Badia-i-Mompel P, Vélez Santiago J, Braunger J, Geiss C, Dimitrov D, Müller-Dott S, et al. decoupleR: ensemble of computational methods to infer biological activities from omics data. Bioinformatics Advances. 2022 Jan 1;2(1):vbac016. doi:10.1093/bioadv/vbac016

52. Yu G. Thirteen years of clusterProfiler. The Innovation. 2024 Nov;5(6):100722. doi:10.1016/j.xinn.2024.100722

53. Derr A, Yang C, Zilionis R, Sergushichev A, Blodgett DM, Redick S, et al. End Sequence Analysis Toolkit (ESAT) expands the extractable information from single-cell RNA-seq data. Genome Res. 2016 Oct 1;26(10):1397–410. doi:10.1101/gr.207902.116

54. Korsunsky I, Millard N, Fan J, Slowikowski K, Zhang F, Wei K, et al. Fast, sensitive and accurate integration of single-cell data with Harmony. Nat Methods. 2019 Dec;16(12):1289–96. doi:10.1038/s41592-019-0619-0

925 55. Aibar S, González-Blas CB, Moerman T, Huynh-Thu VA, Imrichova H, Hulselmans G, et al.
926 SCENIC: single-cell regulatory network inference and clustering. Nat Methods. 2017
927 Nov;14(11):1083–6. doi:10.1038/nmeth.4463

928 56. Herrera-Uribe J, Wiarda JE, Sivasankaran SK, Daharsh L, Liu H, Byrne KA, et al. Reference
929 Transcriptomes of Porcine Peripheral Immune Cells Created Through Bulk and Single-Cell RNA
930 Sequencing. Front Genet. 2021 Jun 23;12:689406. doi:10.3389/fgene.2021.689406

931 57. Paradis E, Schliep K. ape 5.0: an environment for modern phylogenetics and evolutionary analyses
932 in R. Schwartz R, editor. Bioinformatics. 2019 Feb 1;35(3):526–8.
933 doi:10.1093/bioinformatics/bty633

934 58. Posit team. RStudio: Integrated Development Environment for R [Internet]. Boston, MA: Posit
935 Software, PBC.; 2025. Available from: http://www.posit.co/

936 59. Samuel Marsh, Maëlle Salmon, Paul Hoffman, kew24, Mustafa Samet Pir. samuel-
937 marsh/scCustomize: Version 3.2.0 [Internet]. Zenodo; 2025 [cited 2025 Dec 9]. Available from:
938 https://zenodo.org/doi/10.5281/zenodo.17094431 doi:10.5281/ZENODO.17094431

939 60. Wickham H. ggplot2: elegant graphics for data analysis. Second edition. Switzerland: Springer;
940 2016. 260 p. (Use R!). doi:10.1007/978-3-319-24277-4

941 61. Gu Z. Complex heatmap visualization. iMeta. 2022 Sep;1(3):e43. doi:10.1002/imt2.43

Figure 1

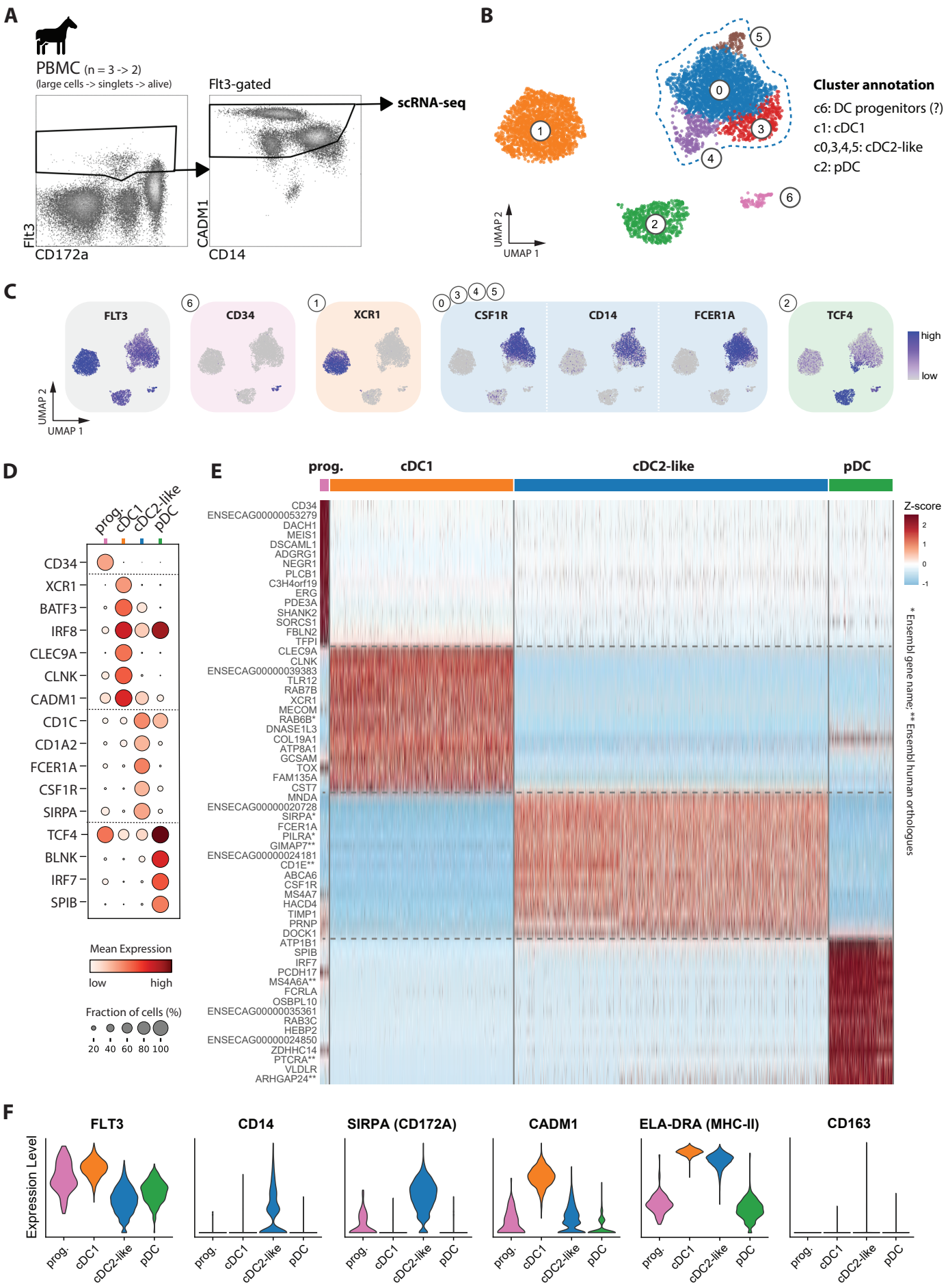

Figure 1: Identification of main DC subsets in equine blood by scRNA-seq. (**A**) Gating strategy to enrich DC from equine PBMC for scRNA-seq by FACS (large cells/singlets/alive/Flt3^{+}CADM1$^{+/hi}$). (**B**) UMAP plot with annotation of putative DC progenitors, cDC1, cDC2-like cells, and pDC. (**C**) Feature plots of key markers used for subset identification. (**D**) Dotplot with additional DC subset-specific genes. (**E**) Heatmap with top 15 differentially expressed genes. Complete lists are given in **Supp. Table 1**. (**F**) Violin plots show transcript expression for phenotypic markers previously analyzed by flow cytometry.

Figure 2

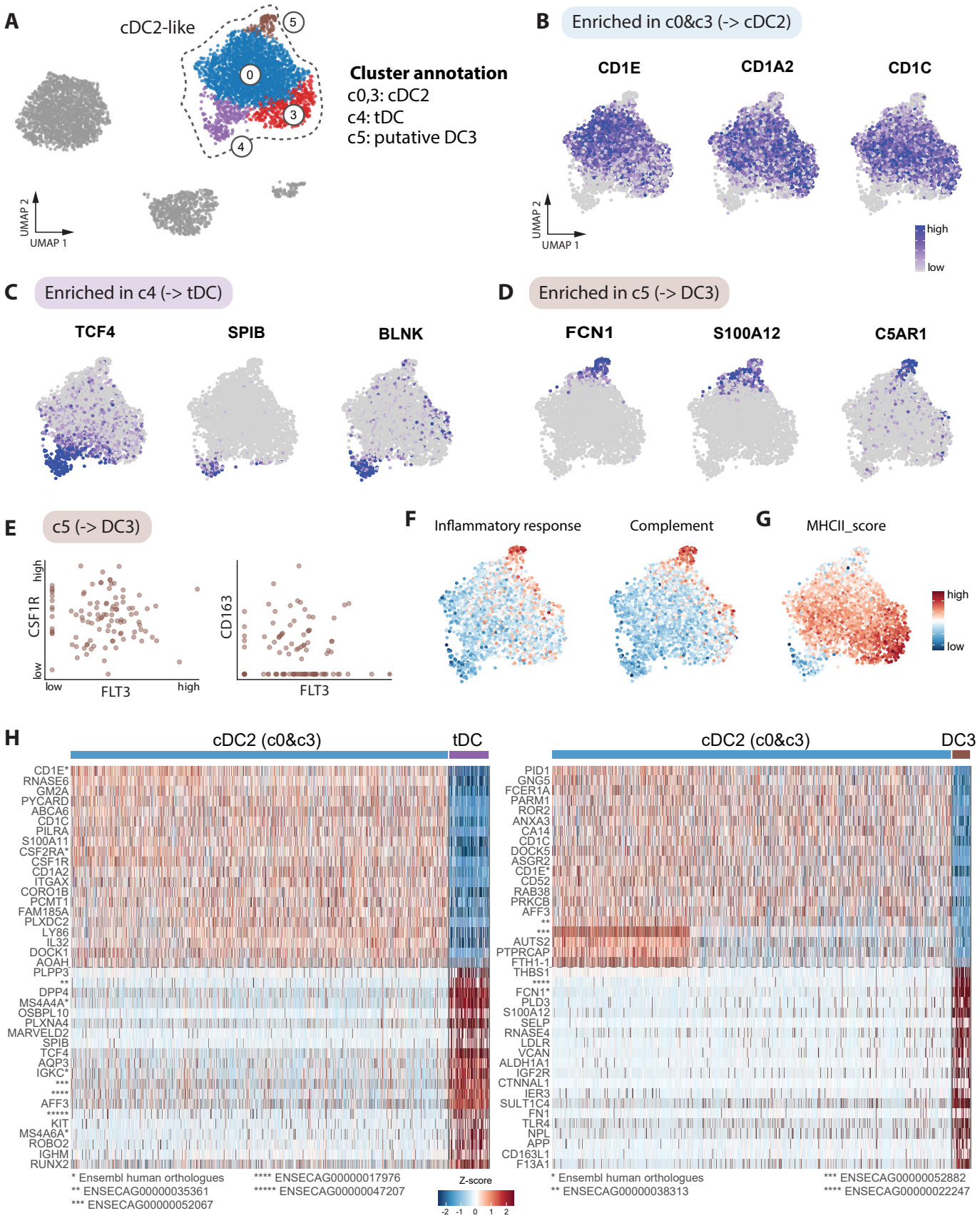

Figure 2: Delineation of tDC and putative DC3 from cDC2. (**A**) Annotation of cDC2-like clusters in UMAP plot. (**B**) Feature plots show expression of CD1 genes, enriched in cDC2. (**C**) Feature plots show expression of pDC-related genes, enriched in tDC. (**D**) Feature plots show expression of pro-inflammatory genes (*FCN1*, *S100A12*, *C5AR1*), enriched in DC3 (c5). (**E**) Scatter plots show co-expression of *FLT3* and monocyte markers (*CSF1R*, *CD163*) at the single-cell level in cluster 5 (DC3). (**F**) Feature plots of cDC2-like cells showing module scores for the Hallmark gene sets “inflammatory response” and “complement”. (**G**) Feature plot of cDC2-like cells showing MHC-II score (custom gene module, see **M&M**). (**H**) Heatmaps showing top 20 DEGs from pairwise comparisons between cDC2 (c0&c3) and tDC on the left, and between cDC2 (c0&c3) and DC3 on the right. Complete gene lists are given in **Supp. Table 2**.

Figure 3

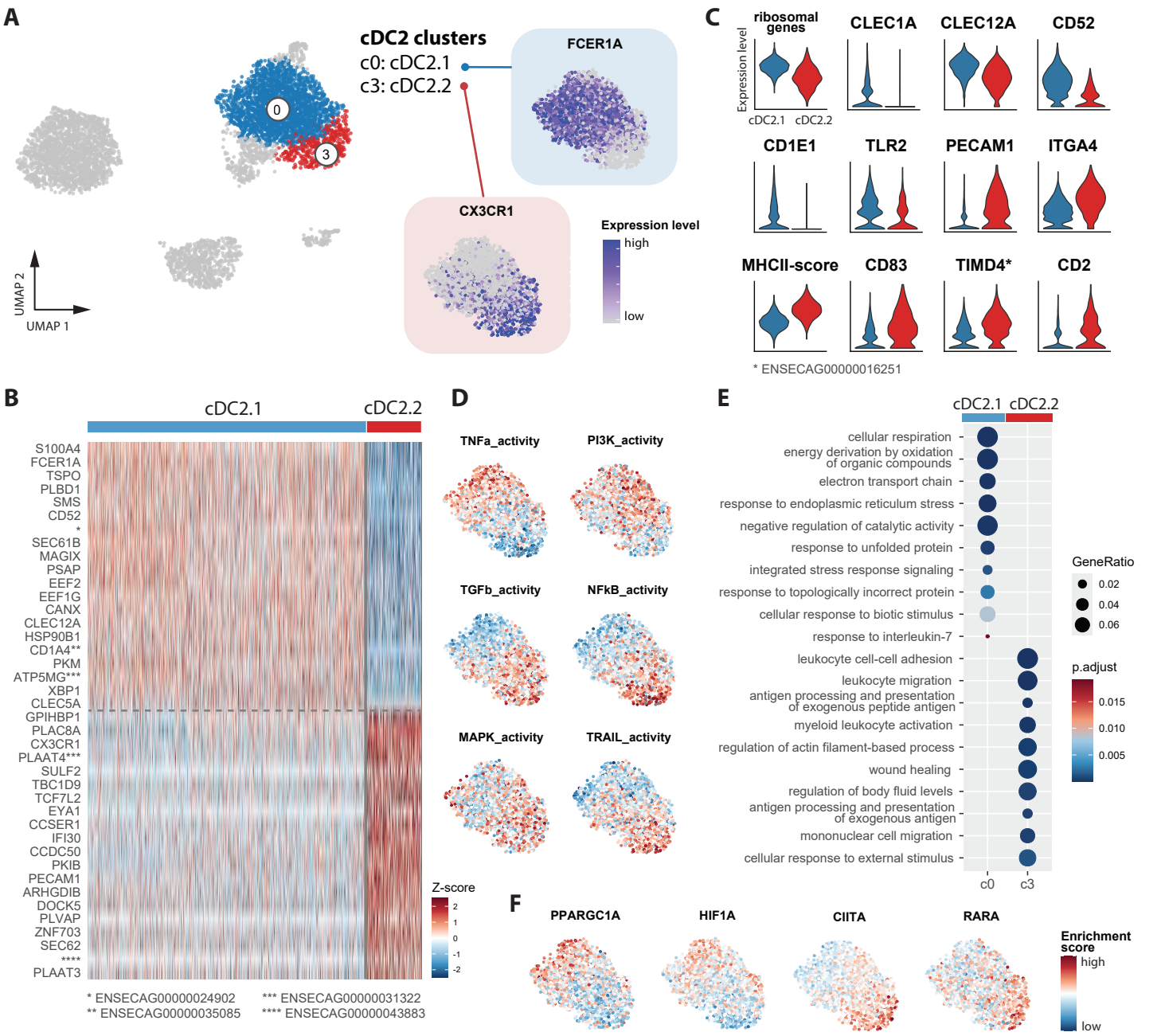

Figure 3. Heterogeneity of cDC2. (**A**) Annotation of cDC2 subsets (cDC1.1, cDC2.2) in UMAP plot and their expression of *FCER1A* and *CX3CR1* visualized in feature plots. (**B**) Heatmap displays top 20 differentially expressed genes (DEGs) between cDC2 subsets. Complete gene lists are given in **Supp. Table 3**. (**C**) Violin plots show selected DEGs between cDC2 subsets. (**D**) Feature plots show inferred regulatory activity scores for selected PROGENy pathways across the two cDC2 clusters. (**E**) Dot plot illustrates selected enriched Gene Ontology (GO) biological process terms in the two cDC2 clusters, as determined by over-representation analysis. (**F**) Feature plots show inferred regulatory activity scores for selected differentially regulated transcription factors (TF) across the two cDC2 clusters. Complete TF list is given in **Supp. Table 3**.

Figure 4

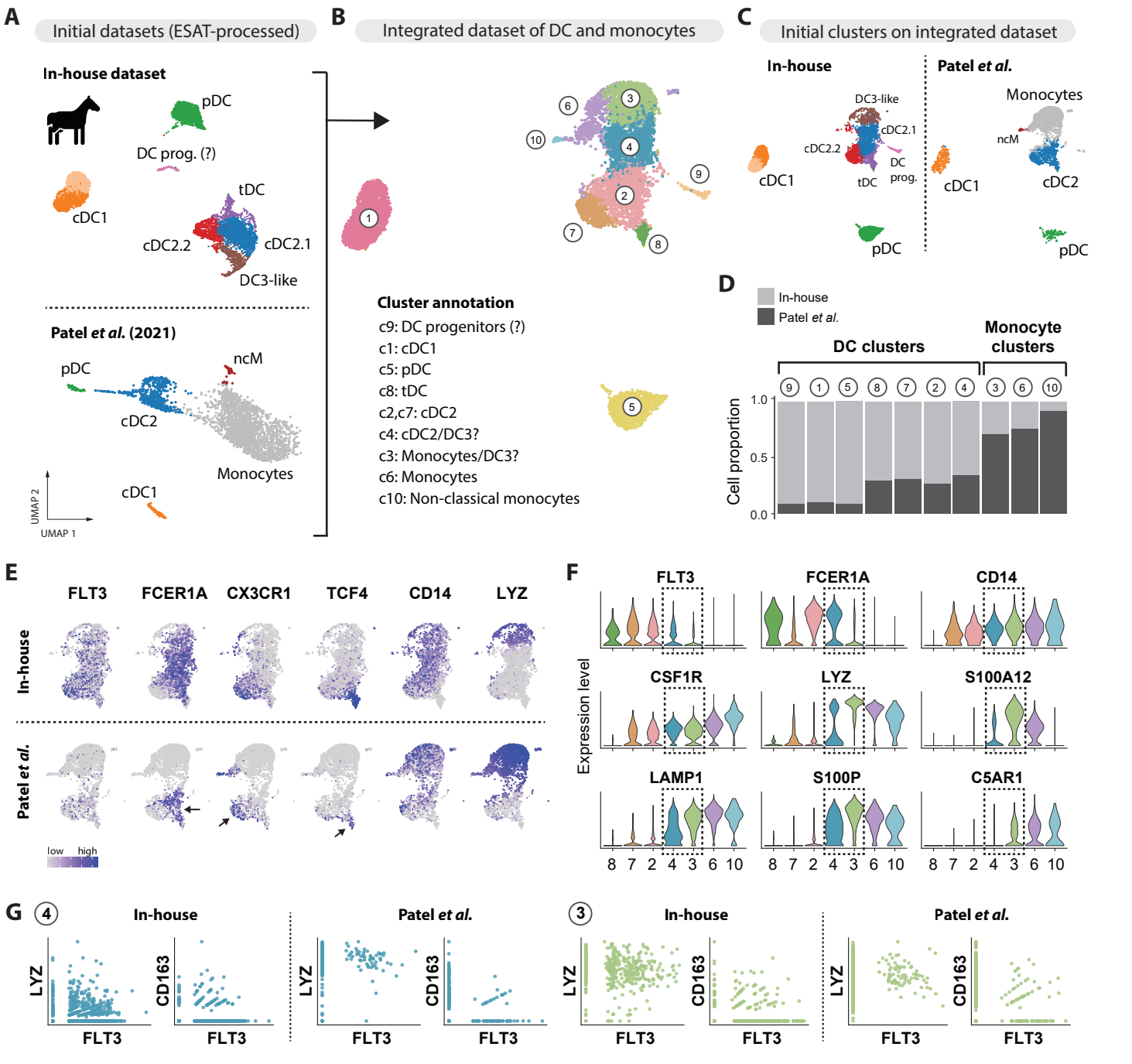

Figure 4: Challenges in delineating DC from monocytes. (**A**) Our in-house dataset (enriched equine DC) was re-processed according to Patel *et al.* and integrated with DC and monocytes from this previously published dataset (Patel *et al.*, equine PBMC). (**B**) UMAP plot shows annotation of ten clusters in integrated dataset. (**C**) UMAP plots show location of initial clusters (depicted in **Fig. 4A**) on integrated dataset. (**D**) Bar plots show contributions (cell proportions) of initial datasets (in-house vs. Patel *et al.*) to clusters in integrated dataset. (**E**) Key marker genes visualized in feature plots on the integrated UMAP, split by dataset (in-house vs. Patel *et al.*). (**F**) Key marker genes visualized as violin plots for clusters in integrated dataset. Clusters 4 and 3 were highlighted by dashed frames. (**G**) Scatter plots illustrate co-expression of *FLT3* and *LYZ* or *CD163* in cells of cluster 4 (blue) and cluster 3 (green) by dataset (in-house vs. Patel *et al.*).

Figure 5

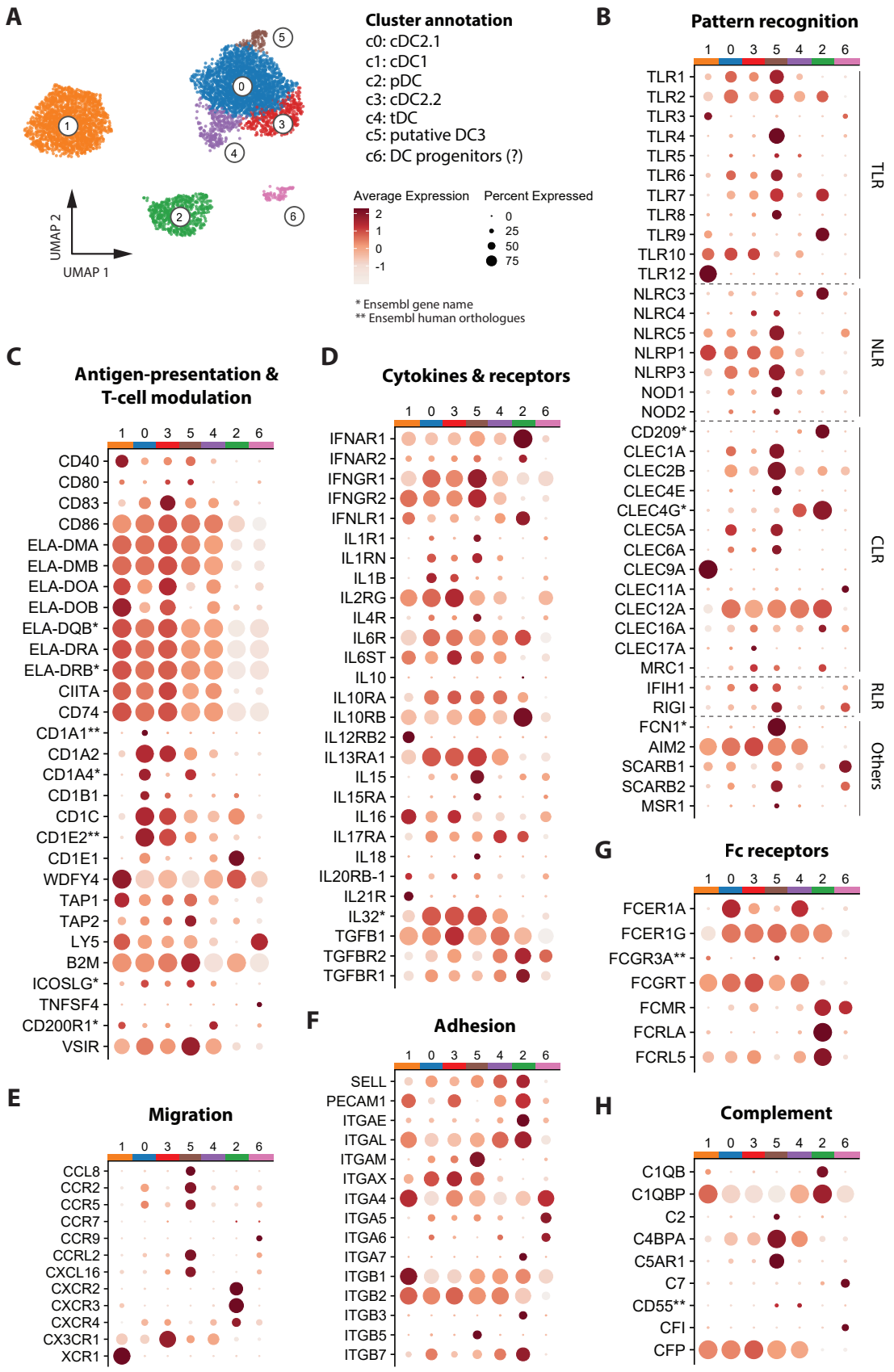

Figure 5: Gene expression related to main DC functions. (**A**) Cluster annotation. (**B-H**) Dot plots visualize gene expression across all annotated clusters related to pattern recognition (**B**), antigen presentation and T-cell modulation **(C)**, cytokines and receptors (**D**), migration (**E**), adhesion (**F**), Fc receptors (**G**) and complement (**H**).

Figure 6

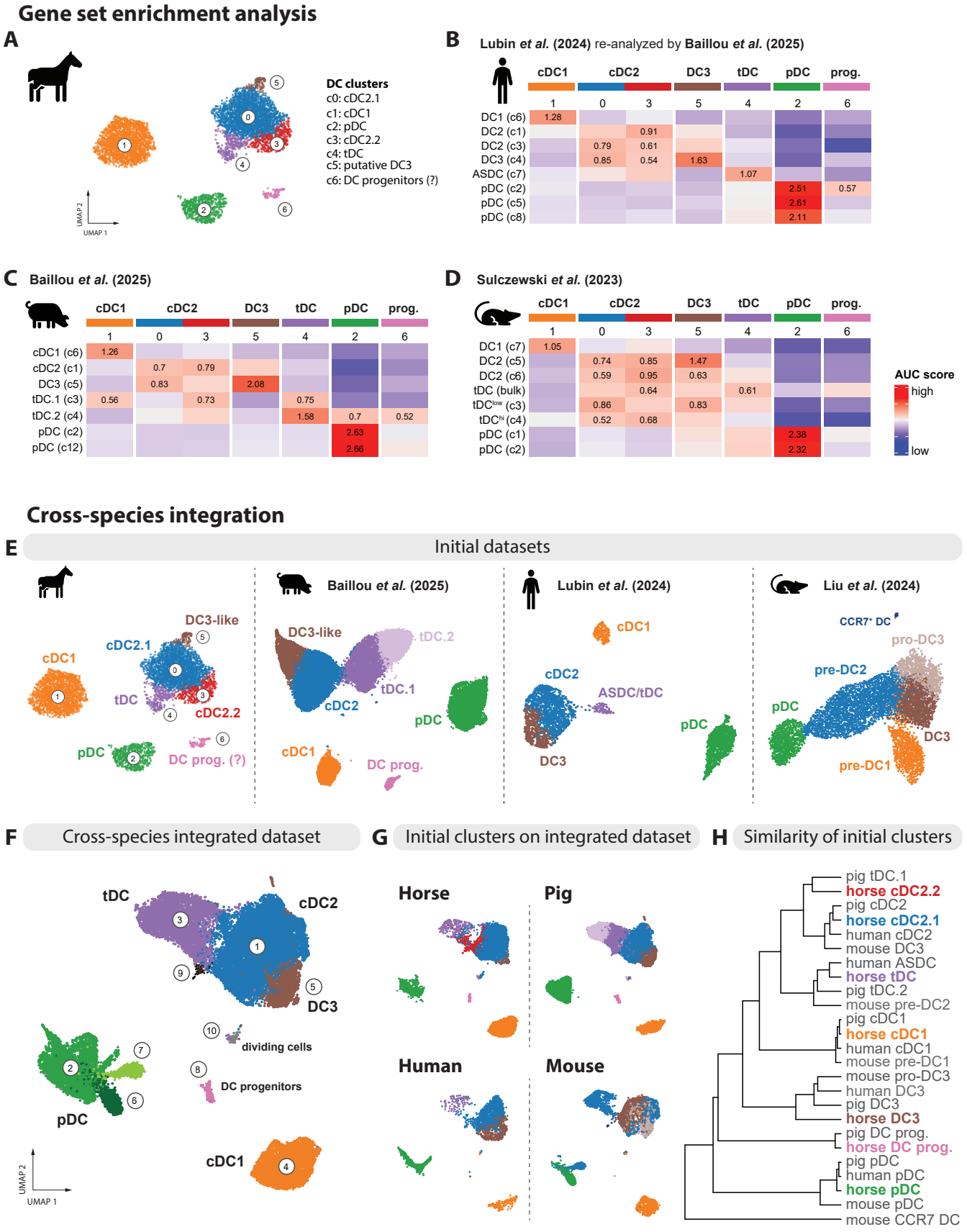

Figure 6: Cross-species comparison of DC subsets. (**A**) UMAP plot showing cluster annotation for equine DC subsets. (**B-D**) Heatmaps showing averaged scaled enrichment scores for gene signatures from porcine blood DC subsets (Baillou *et al.*), from murine splenic DC (Sulczewski *et al.*), and from human blood DC (Lubin *et al.*, re-analyzed by Baillou *et al.*), calculated using the AUC method (see **Supp. Table 4** for gene signatures). AUC relative scores >= 0.5 are displayed. (**E**) Integration of scRNA-seq datasets of blood-enriched DC from horse, pig (Baillou *et al.*), human (Lubin *et al.*, re-analyzed by Baillou *et al.*) and mouse (Liu *et al.*). UMAP plots show initial datasets and their respective cluster annotations. (**F**) UMAP plot showing cluster annotation for cross-species integrated dataset. (**G**) UMAP plots showing location of initial clusters (depicted in **Fig. 6E**) on integrated dataset. (**H**) Similarity tree showing correlations between the initial species-specific clusters in the integrated dataset, calculated using Euclidean distances.